KAUNAS UNIVERSITY OF TECHNOLIGY

FACULTY OF MECHANICAL ENGINEERING AND DESIGN

Neringa Kraptavičiūtė

THE EXPERIMENTAL AND NUMERICAL STUDY OF INCUS

Final Project of Master's degree

Supervisor
dr. Virginija Gylienė

KAUNAS, 2017

KAUNO TECHNOLOGIJOS UNIVERSITETAS

MECHANIKOS INŽINERIJOS IR DIZAINO FAKULTETAS

Neringa Kraptavičiūtė

EKSPERIMENTINIS IR SKAITINIS AUSIES PRIEKALO TYRIMAS

Baigiamasis magistro projektas

Vadovė
dr. Virginija Gylienė

KAUNAS, 2017

KAUNAS UNIVERSITY OF TECHNOLOGY

FACULTY OF MECHANICAL ENGINEERING AND DESIGN

PRODUCTION ENGINEERING DEPARTMENT

THE EXPERIMENTAL AND NUMERICAL STUDY OF INCUS

Final Project of Master's degree

Production Engineering (Code 621H70004)

Supervisor
dr. Virginija Gylienė

Reviewer
Assoc. prof. Giedrius Janušas

Project made by
Neringa Kraptavičiūtė

KAUNAS, 2017

KAUNAS UNIVERSITY OF TECHNOLOGY

FACULTY OF MECHANICAL ENGINEERING AND DESIGN
(Faculty)

NERINGA KRAPTAVIČIŪTĖ
(Name, Surname of the student)

PRODUCTION ENGINEERING (Code 621H70004)
(Study programe, code)

"The experimental and numerical study of incus"

DECLARATION OF ACADEMIC INTEGRITY

20 ____ m. _____ _____ d.
Kaunas

I confirm that the final project of mine, Neringa Kraptavičiūtė, on the subject "Experimental and numerical study of incus" is written completely by myself; all the provided data and research results are correct and have been obtained honestly. None of the parts of this thesis have been plagiarized from any printed, Internet-based or otherwise recorded sources. All direct and indirect quotations from external resources are indicated in the list of references. No monetary funds (unless required by law) have been paid to anyone for any contribution to this thesis.

I fully and completely understand that any discovery of any manifestations/cases/facts of dishonestly inevitably results in me incurring a penalty according to the procedure(s) effective at Kaunas University of Technology

(name and surname filled by hand) *(signature)*

KAUNAS UNIVERSITY OF TECHNOLOGY
FACULTY OF MECHANICAL ENGINEERING AND DESIGN

I approove: _____
(parašas, data)

Head of Department _____
(vardas, pavardė)

MASTER STUDIES FINAL PROJECT TASK ASSIGNMENT
Study program: PRODUCTION ENGINEERING

The final project of master's studies aimed to gain the master's qualification degree is a research or applied type project. 30 credits are assigned for its completion and defense. The final project of a student must demonstrate the more profound and extensive knowledge acquired in the main studies as well as the gained skills enabling the student to outline and solve an actual problem when in possession of limited and or contradictory information, to independently conduct scientific or applied analysis and to interpret data properly. By completing and defending the final project of master's studies, a student must demonstrate creativity, ability to apply fundamental knowledge, understanding of social and commercial environment(s), legal acts and financial limitations, to demonstrate information search skills as well as ability to carry out analysis requiring advanced qualification(s), to use quantitative research methods, to apply relevant software, to use common information processing techniques and correct language and to demonstrate the ability of formulating proper conclusions.

1. Title of the Project

The experimental and numerical study of incus

Approved by the Dean on 2016 y. 12 m. 8 d. Order No. V25-11-20

2. Aim of the Project

Perform experimental and numerical study of human incus bone and evaluate its microstructure and mechanical properties as an inverse problem combining eigenfrequency analysis and FE calculations

3. Structure of the Project:

1. Problem analysis.
2. Experimental study of human incus bone.
3. Numerical study of human incus bone.

4. Requirements and conditions

1. Review and analyze Final Project aim related literature.
2. Accomplish visual samples evaluation and mass measurements.
3. Evaluate bone microstructure using results from incus bone μCTomography test.
4. Perform frequency experiment using piezoelectric system.
5. To create three-dimensional computational model and perform eigenfrequencies analysis.

This task assignment is an integral part of the final project.

5. Project submission deadline 2017.12.21

Given to the student _____

Task Assignment received _____ _____

(Name, Surname of the student) (Signature, date)

Supervisor _____ _____

(Name, Surname of the Supervisor) (Signature, date)

Kraptavičiūtė Neringa. Eksperimentinis ir skaitinis ausies priekalo tyrimas; Magistro baigiamasis projektas / vadovė dr. Virginija Gylienė; Kauno technologijos universitetas, Mechanikos inžinerijos ir dizaino fakultetas.

Mokslo kryptis ir sritis: Technologijos mokslai, Gamybos inžinerija

Reikšminiai žodžiai: Baigtinių elementų metodas, mechaninės savybės, klausa, ausies priekalas

Kaunas, 2017.64 p.

SANTRAUKA

Baigtinių elementų metodas plačiai taikomas klausos problemų tyrimuose: nustatant ir identifikuojant audinių savybes, apibūdinant klausos elementų elgesį tam tikromis sąlygomis ar pagerinant chirurginių intervencijų kokybę. Daugybė tyrėjų ir mokslininkų orientuojasi į klausos problemų šalinimo galimybių paiešką ar gilinasi į vidurinės ar vidinės ausies funkcionavimą

Šiame baigiamajame darbe nustatinėjamos ausies priekalo mechaninės savybės. Šiam tikslui pasiekti atlikta mikrotomografijos rezultatų analizė, vibracinė analizė naudojantis pjezoelektrine sistema ir galiausiai sukurtas skaičiuojamasis baigtinių elementų modelis.

Skirtingai nei kitų autorių skaitiniai tyrimai magistro baigiamojo projekto darbo metu sudarytas skaitinis modelis įvertina ausies priekalo nehomogeniškumą. Sudarytas Baigtinių Elementų (BE) modelis su skirtingais tankiais ilgojoje bei trumpojoje kaulo ataugoje. Ilgosios ir trumposios ataugos nehomogeniškumas gali būti viena iš ausies priekalo kaulo nefunkcionavimo priežasčių, kuri tiesiogiai nepriklauso nuo kaulo sunykimo dydžio bei pažeisto kauliuko paviršiaus ploto.

Eksperimentinėje darbo dalyje buvo nustatytas ausies priekalo tankis (atliekant svorio matavimus) bei vibracinė analizė skaitinio modelio validavimui. Naudojant sukurtąjį skaitinį modelį bei atvirkštinį BE modeliavimą galiausiai nustatytas ausies priekalo Jungo modulis.

Kraptavičiūtė Neringa. *The Experimental And Numerical Study Of Incus*: *Master's* thesis in Production Engineering / supervisor dr. Virginija Gylienė Faculty of Mechanical Engineering and Design, Kaunas University of Technology.

Research area and field: Technological sciences, Production Engineering

Key words: Finite Element Modelling, mechanical properties, hearing, incus.

Kaunas, 2017. 64 p.

SUMMARY

The capabilities to apply the FEM in hearing research field are large: the identification of tissues properties, the definition of the behavior of hearing elements or even it could improve the clinical surgical intervention. Numerous researchers are focused on hearing improvement or understanding problems by working on middle ear or inner ear behavior.

In this Final Project focused on mechanical properties identification of incus by using micro-CT scanning, performing vibrational analysis and finally the FE simulations.

Contrarily to other researchers in this Final Project was supposed that incus bone to be non-homogeneous body and accordingly attributed different densities in long and short processes. The non-homogeneity of the long and short processes could be the reason why the incus bone behavior does not depend simply on degradation level and affected area size.

From experimental study of incus bone performing mass measurements was estimated bone volume. Also, was performed modal analysis of numerical model for validation. Finally, using incus bone numerical model by inverse FE modelling, the Young Modulus was estimated.

TABLE OF CONTENTS

INTRODUCTION 9

1. PROBLEM ANALYSIS 10

1.1. HUMAN HEARING SYSTEM 10

1.2. OSSICLES 11

1.3. HEARING DISEASES 12

2. EXPERIMENTAL STUDY OF INCUS 14

2.1. SAMPLE PREPARATION 15

2.2. SAMPLES MASS MEASUREMENT 18

2.3. EVALUATION OF INCUS MICROSTRUCTURE 22

2.4. FREQUENCY EXPERIMENT 28

3. NUMERICAL STUDY OF INCUS 31

3.1. COMPOSITION OF FINITE ELEMENT MODEL OF INCUS 31

3.2. CONVERGENCE ANALYSIS 36

3.3. DISPLACEMENT ANALYSIS 40

3.4. YOUNG'S MODULUS IDENTIFICATION 42

CONCLUSIONS 45

RECOMMENDATIONS 46

REFERENCES 48

APPENDIX 9

I. THE COVER PAGE OF PUBLISHED ARTICLE 51

II. DISPLACEMENT DIAGRAMS 53

I.I. LINEAR ELEMENT TYPE 53

I.II. QUADRATIC ELEMENT TYPE 59

INTRODUCTION

One of the most important senses for human - is hearing. Hearing problems affect life quality and emotional state. All over the world more than 500 million people has hearing problems (1).

The mechanism of hearing involves conduction of mechanical vibrations along the ossicular chain to the inner ear (2). The middle ear system with its smallest bones and articulations is responsible for catching noise energy and transforming it to perilymph pressure changes in the cochlea. Of the three ossicles from the middle ear, the incus was often reported in literature to be the most eroded bone and the more distant from the inflammation focus (3) (4). Also from ossicles' surgery the surgeons observed that incus bone work does not depend on degradation level and affected area size. It can be assumed, that this is influenced by the incus bone microstructure.

The aim of this Final Project is to perform experimental and numerical study of human incus bone and evaluate its microstructure and mechanical properties as an inverse problem combining eigenfrequency analysis and FE calculations. To achieve this goal is necessary to perform following tasks:

1. Review and analyse Final Project aim related literature.
2. Accomplish visual samples evaluation and mass measurements.
3. Evaluate bone microstructure using results from incus bone μCTomography test.
4. Perform frequency experiment using piezoelectric system.
5. To create three-dimensional computational model and perform eigenfrequencies analysis.

The problem mentioned above is relevant, because well knowing incus bone mechanical properties and microstructure would be easier to adapt and to create middle ear bone implants and reconstruct human hearing system.

1. PROBLEM ANALYSIS

1.1. HUMAN HEARING SYSTEM

Human ear is the hearing and balance organ. It is divided in to three parts – outer ear, middle ear and inner ear (*Fig. 1.1*). Outer ear and the middle ear are associated only with the audio sensing, and in the inner ear sound and balance receptors are located (5).

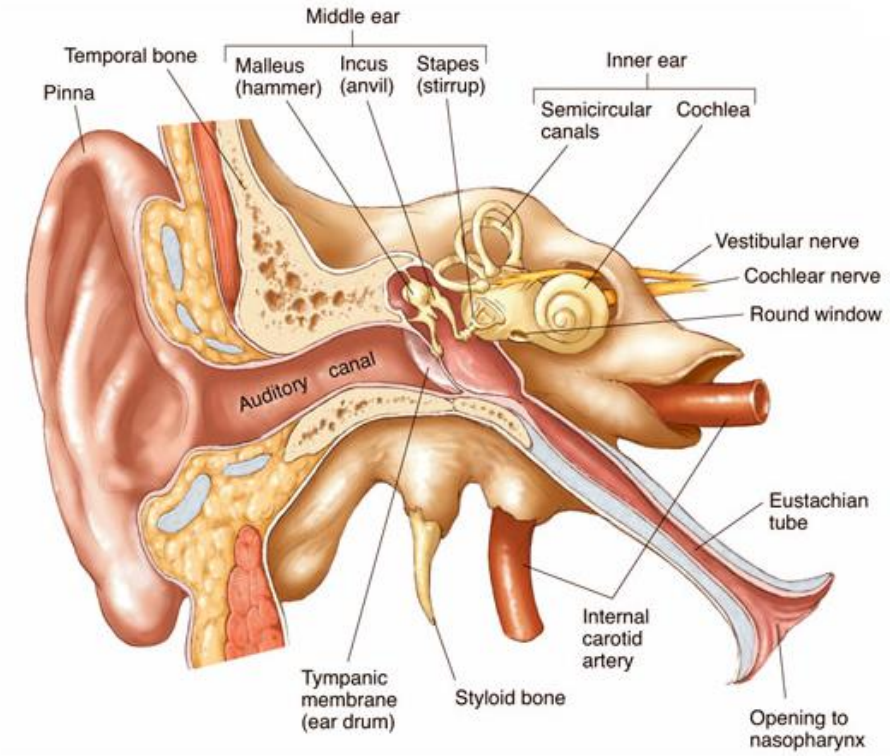

Fig. 1.1 Human hearing system (6)

Outer ear (lat. Auris externa) consists of pinna and the auditory canal. It gathers sound energy and focuses it on the eardrum (tympanic membrane).

Middle ear (lat. Auris media) consists of tympanic cavity, three tiny bones known as ossicles and auditory tube. The primary function of the middle ear is to offset the decrease in acoustic energy that would occur if the low impedance ear canal air directly contacted the high-impedance cochlear fluid (7).

Inner ear (lat. Auris interna) consists of cochlea, the balance mechanism, the vestibular and the auditory nerve.

Human receptors distinguish sound of air vibrations with, in a frequency range 20 – 20000 Hz (5). Sound waves vibrate the eardrum. Ossicles, which are attached to the eardrum, strengthen sound waves and transmit the vibrations to the membrane of the vestibular nerve. Then in the cochlea sound waves are converted to nervous impulses which via auditory nerve, are transmit to the brain.

1.2. OSSICLES

As it was mentioned above, middle ear includes three bones (lat. Ossicula auditus) – hammer (lat. *Malleus*), anvil (lat. *Incus*) and stirrup (lat. *Stapes*) (F*ig.1.2*). They are the smallest bones in the human body (5). The ossicular chain connects the tympanic membrane and the inner ear, and plays an important role in amplifying and regulating sound waves (8)

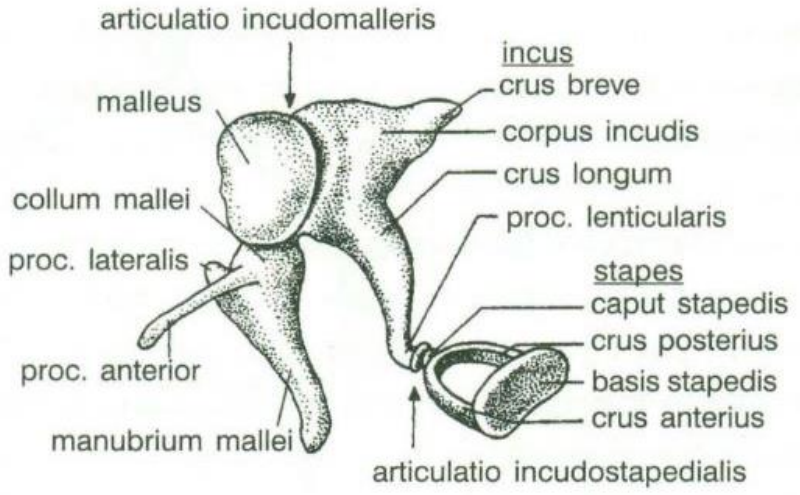

Fig.1.2 Ossicles (5)

The hammer articulates with the incus through the incudomalleolar joint and is attached to the tympanic membrane, from which vibrational sound pressure motion is passed. The anvil bone consists of body and short and long processes. Long process is connected with stirrup. Stirrup bone consists of head, anterior crus, posterior crus and a base. Stirrup head makes joint with anvil and a base covers the oval window (5). In doing so the spatial motion of the ossicular chain appears as the one of main causes of the hearing quality (9).

1.3. HEARING DISEASES

Ear inflammation and other ear diseases are common problems that affect people's ability to hear. There are estimated 27 million people in China with hearing loss. Worldwide, the number is estimated to be more than 500 million (1). The degree of ossicular chain deterioration or damage in humans, as a result of inflammatory disease, trauma or malformation, is variable (10). Hearing loss can be caused by many different reasons, some of which can be successfully treated with medicine or surgery, depending on the disease process. There are three different types of hearing loss (11):

1. Conductive hearing loss - when hearing deficit is due to problems with the ear canal, ear drum, or middle ear and its little bones (the malleus, incus, and stapes).
2. Sensorineural hearing loss (SNHL) - when hearing deficiency is due to problems of the inner ear, also known as nerve-related hearing loss.
3. Mixed hearing loss - refers to a combination of conductive and sensorineural hearing loss. This means that there may be damage in the outer or middle ear and in the inner ear (cochlea) or auditory nerve.

Hearing deterioration can occur for a variety of reasons such as high noise level (eg. fireworks, constant work in noisy environments, loud music, etc.), head trauma, autoimmune inner ear disease, various medicines using, after infectious diseases such as influenza, meningitis, hepatiti) (12).

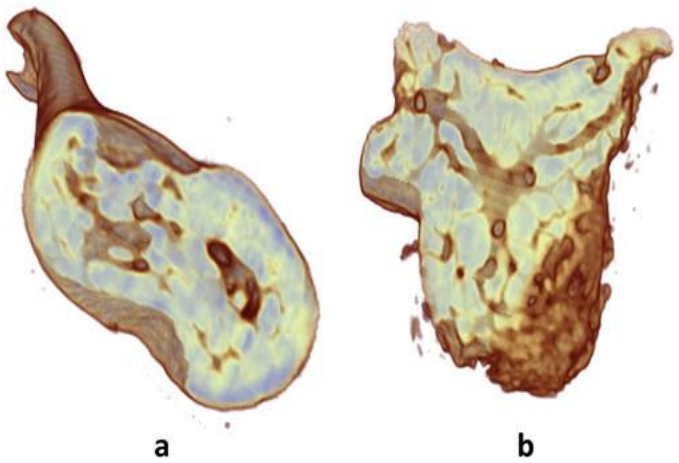

Fig.1.3 Incus bone; image from the micro scanner survey: a – non-inflammatory incus; b – inflammatory incus (4)

Group of French scientists did a research, and found that damaged incus bone structure is changed (4). They compared 15 healthy bones with 13 damaged ones. To identify the bone structure, they used μCTomograph. It was found that incus bone is cortical in nature with a cavity in

its middle part. The comparison of the healthy and damaged bones showed that damaged bones are characterized by strong degradation level and increase of porosity (*Fig. 1.3*)

Borgstein et al (13) highlighted, that the problem of erosion of the incus is a frequently observed, but rarely discussed problem. Park (14) also examined the problems of the long process of incus but caused by congenital origin. Finally, Yung (15) summarised ossicular damage in the patients with atelectasis and found that for 72% of cases in posterior retraction pocket only incus was eroded.

It is hypothesised that the function of the malleus-incus-stapes arrangement is to link the drum to the oval window with the flexibility required for impedance matching but the rigidity to prevent unconstrainable resonances from occurring in the hearing range (2). If it is true, then the structural stiffness of ossicular chain is the critical design for middle-ear replacement prostheses.

Nevertheless, the substituting materials should fit according to the material characteristics; the geometrical requirements are also important. Kaftan et al (10) accentuate that the most difficult situation is to evaluate the length of prosthesis. For this kind of problems, and others, the finite element method (FEM) has distinct advantages in modelling complex biological systems when compared to other techniques (16). Even, as reported in (17) it could improve the clinical surgical intervention.

Consecutively to ossicles' surgery the surgeons observed that incus bone work does not depend on degradation level and affected area size. They observed that sometimes damaged bone part is large but it does not affect bone work in whole hearing system; and opposite – the bone degradation level can be low but the ossicles not functioning. Also, it is important to mention, that there is no method how to identify bone degradation level before surgery – surgeons evaluate osccicles condition and decide necessity to change them only after ear opening.

From these observations, a hypothesis could be made that this phenomenon is affected by the bone microstructure, segmentation and porosity. Also, it can be supposed that location of the focus of infection also affects bone strength and its ability to transmit vibrations. To confirm or to deny this hypothesis was decided to perform experimental and numerical study of Incus.

2. EXPERIMENTAL STUDY OF INCUS

Firstly, a study of the middle ear bone incus microstructure and mechanical properties was undertaken. An example of the study object is shown in *Figure 2.1*. Dimensions (L x W x H) of the sample is 4.564 x 4.247 x 5.641 mm. To identify bone microstructure μCTomograph was used, to evaluate bone porosity, and to identify bone type – cortical (compact) or trabecular (porous). To identify real value of incus bone Young's Modulus was performed frequency analysis using piezoelectric system.

Fig.2.1 Study object

Four incus bones were prepared for this study. Each incus bone was removed due to surgical treatment. Also, each sample was coded to 1M, 1V, 18ZV and 1VS (Fig.2.2) for the privacy of patients.

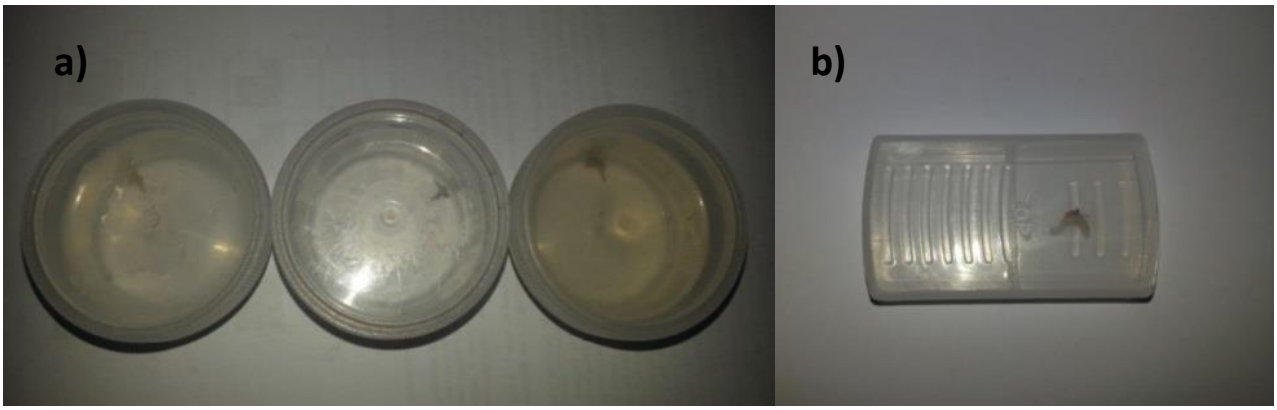

Fig.2.2 Study objects: a) Incus bone samples in formaldehyde; b) Incus bone sample in dry box

Table 2.1 Bone samples

Sample name	Gender	Age, years
1M	Female	63
1V	Male	15
18ZV	Male	18
1VS	Male	13

Three of the samples – *1V, 1M, 18ZV* – were kept in recipients containing fluid (formaldehyde) and one – *1VS* – was kept in box without liquid. All incuses were obtained from four patients – three male (age range: 13 – 18 years) and one female (age: 63 years) (*Table 2.1*).

2.1. SAMPLE PREPARATION

All four samples were kept in refrigerator in about +5^{o} C temperature. Samples were taken of the refrigerator only for experiments and after tests put back to it.

After removing them of refrigerator, samples kept in formaldehyde were taken from solution and put on the paper towel to dry (*Fig.2.3*).

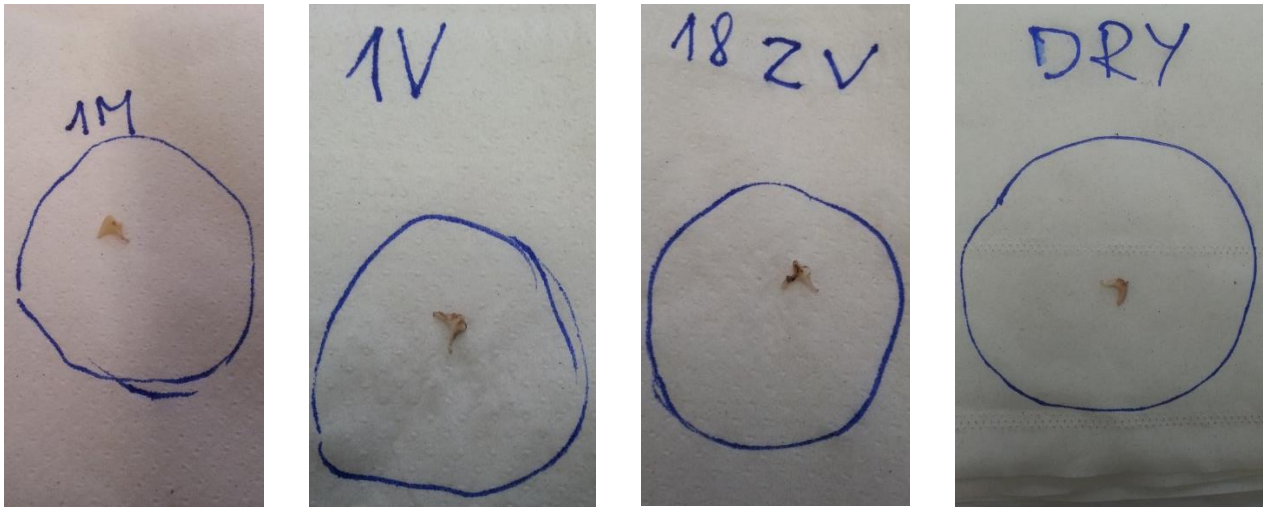

Fig.2.3 Samples *1M, 1V, 18ZV, DRY* (*1VS*) before visual inspection and residual soft tissue removal

After 30 minutes using optical microscope ZEISS® with magnification of 20 (*Fig. 2.4*), all samples were visually inspected to identify their condition. During visual inspection all post-surgery residual soft tissues were removed using tweezers.

Fig.2.4 Microscope used for visual inspection

After visual inspection, it was found that the most infection damaged and the sickliest incus was the sample *18ZV*. As we can see in F*ig. 2.5*, the infection damaged the very large part of the incus body, but the external aspect of short and long processes seemed to be healthy.

Fig.2.5 Incus bone – sample 18ZV image when viewed through a microscope (x20)

1VS sample was identified as the second most damaged one. As we can see in *Fig. 2.6*, sample infection damaged mainly incus body and malleus-joint surface.

Fig.2.6 Incus bone – sample 1VS image when viewed through a microscope (x20)

The third by the level of damage is the *1V* sample. It is clearly visible in F*ig. 2.7*, that in this case infection damaged short and long processes and a small part of the body external surface.

Fig.2.7 Incus bone – sample 1V image when viewed through a microscope (x20)

Finally, as it can be observed in *Fig.2.8*, it was found that the less damaged is the *1M* sample.

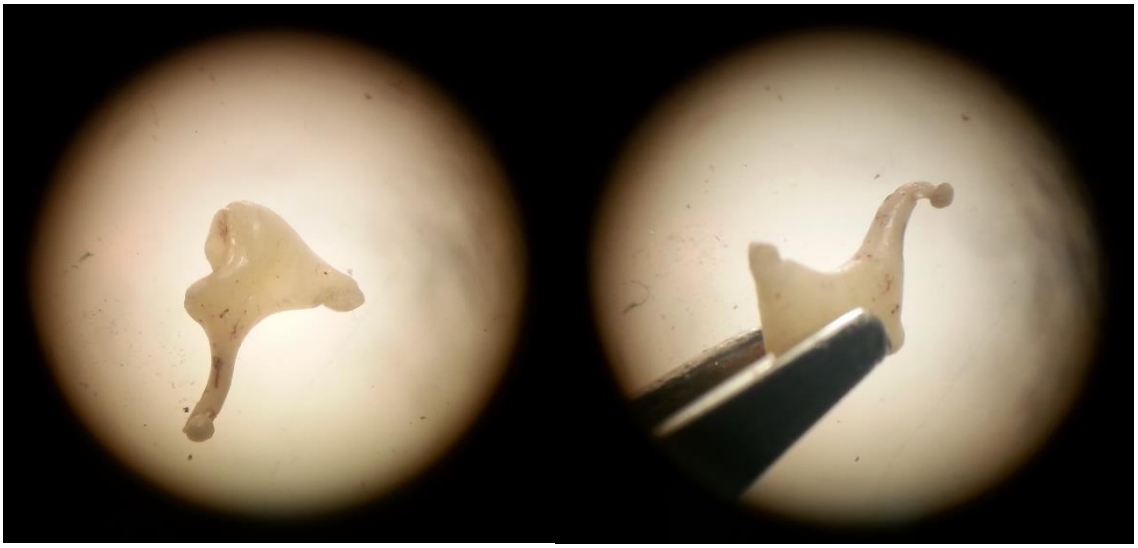

Fig.2.8 Incus bone – sample 1M image when viewed through a microscope (x20)

The picture above shows that *1M* sample has a small groove in the short process. The origin of this groove is unclear, but it was established that this groove is not a result of bone pathology and was not caused during surgery. Some damages can be observed in the long process of this sample, but these alterations are small comparing with other samples.

2.2. SAMPLES MASS MEASUREMENT

After visual inspection with optical microscope, all samples were left to dry at room temperature and controlled humidity. Their mass was measured immediately after the microscopy (t=0 h) then 3 and 8 hours later. For each sequence, the measurements were repeated three times in a row. The high precision balance SARTORIUS CPA225D was used to perform these mass evaluations. The precision *d* of this balance is $d = 0.01\ mg$ for $m < 100\ g$ and $d = 0.1\ mg$ for $100 < m < 220$ g (F*ig. 2.9*).

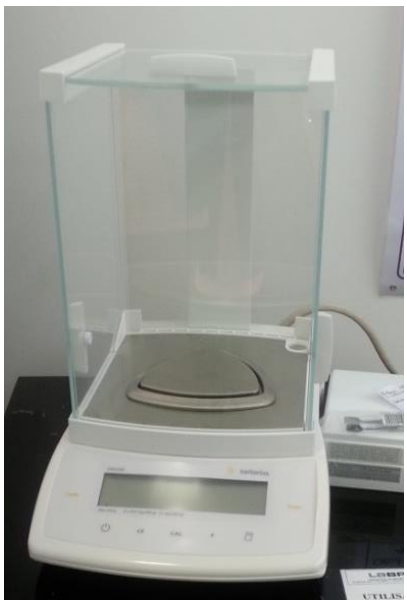

Fig.2.9 Balance SARTORIUS CPA225D used for mass evaluations

The measurement results for samples *18ZV*, *1V* and the *1VS* are summarized in *Table 2.2*, *Table 2.3*, and *Table 2.4*. *Figure 2.10* illustrates their average mass evolution as a function of time.

Table 2.2 Sample 1VS mass measurement

Sample: *1VS*				
Time, h	**Mass (I), g**	**Mass (II), g**	**Mass (III), g**	**Average, g**
0	0.01574	0.01574	0.01574	0.01574
3	0.01587	0.01588	0.01592	0.01589
8	0.01576	0.01581	0.01582	0.01580

Table 2.3 Sample 18ZV mass measurement

Sample: *18ZV*				
Time, h	**Mass (I), g**	**Mass (II), g**	**Mass (III), g**	**Average, g**
0	0.01519	0.01519	0.01519	0.01519
3	0.01536	0.01532	0.01538	0.01535
8	0.01524	0.01526	0.01527	0.01526

Table 2.4 Sample 1V mass measurement

Sample: *1V*				
Time, h	**Mass (I), g**	**Mass (II), g**	**Mass (III), g**	**Average, g**
0	0.01296	0.01296	0.01296	0.01296
3	0.01348	0.01346	0.0135	0.01348
8	0.01334	0.01333	0.01332	0.01333

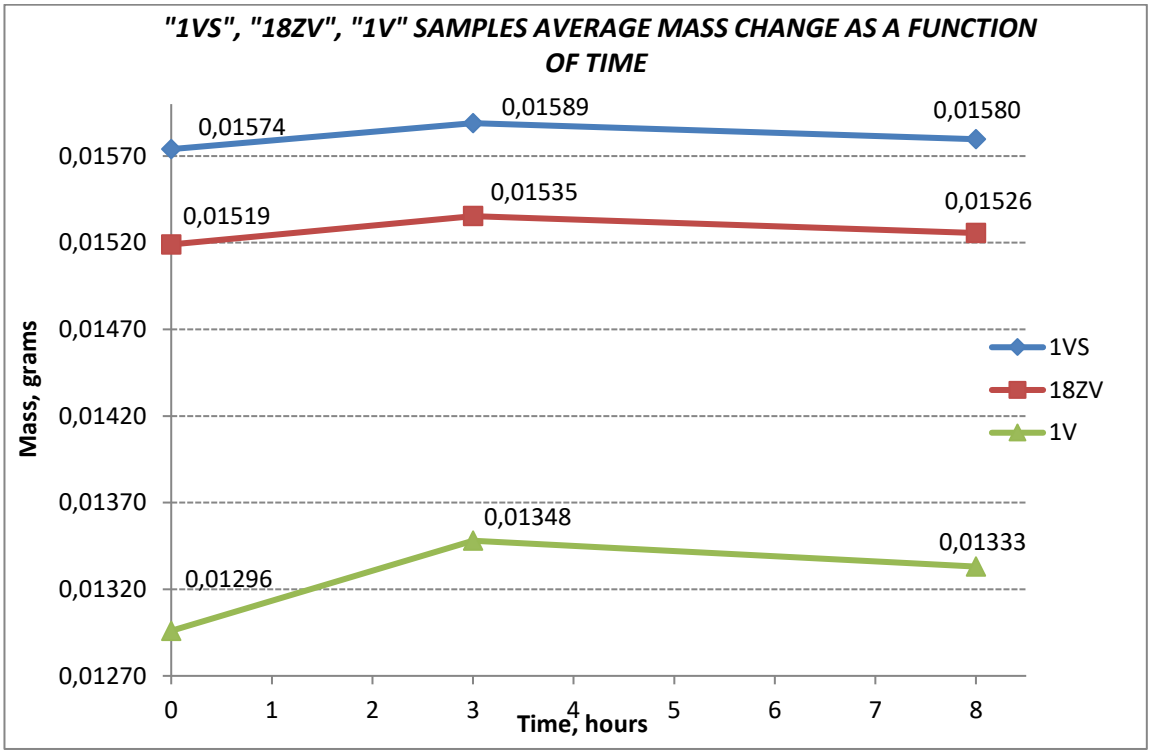

Fig.2.10 *1VS*, *18ZV* and *1V* samples average mass change as a function of time

The tendency of minor mass increase was observed during 3 hours, especially for the sample *1V*, followed by its slow decrease. However, this mass variations are only about 0.05 – 0.1% for each sample.

It may be concluded that mass changes are probably due to the ambient humidity variations and cannot be associated with the formaldehyde evaporation or loss because similar behaviour was observed for dry and humid bone samples.

The same mass measurement experiment was done with *1M* incus. All measurement results are presented in *Table 2.5*.

Table 2.5 Sample *1M* mass measurement

Sample: *1M*				
Time, h	**Mass (I), g**	**Mass (II), g**	**Mass (III), g**	**Average, g**
0	0.02901	0.02901	0.02901	0.02901
3	0.02897	0.02905	0.02900	0.02901
19	0.02871	0.02873	0.02879	0.02874
26	0.02876	0.02875	0.02876	0.02876
93	0.0288	0.02881	0.02883	0.02881
98	0.02878	0.02881	0.02883	0.02881

As for other samples, samples mass was measured immediately after removal from the refrigerator and from formaldehyde solution. However, five supplementary measurements were made after 3, 19, 26, 93 and 98 hours. All results are plotted in F*igure 2.11*.

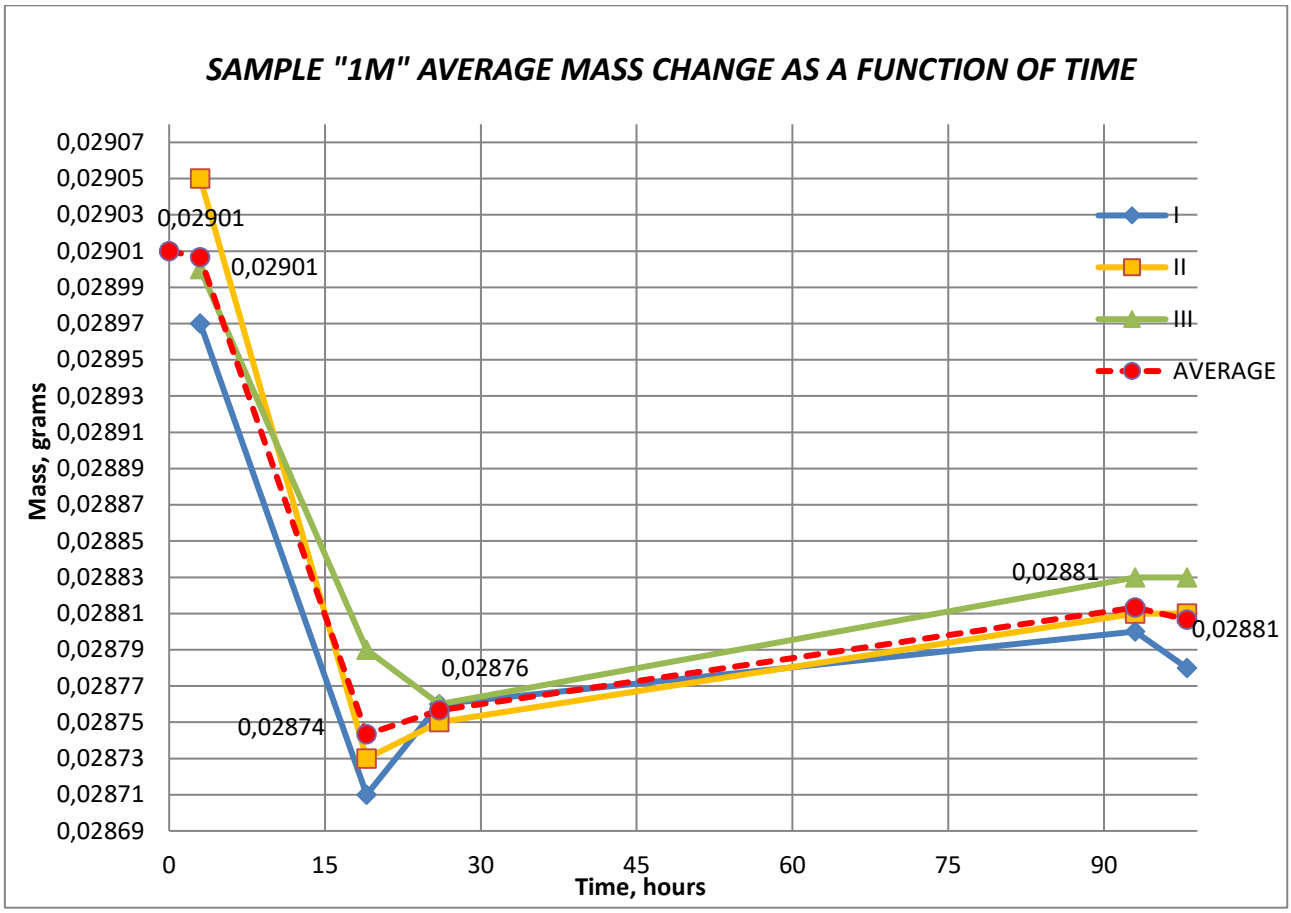

Fig.2.11 Sample *1M* average mass change as a function of time

The results indicate that the mass variation for sample *1M* is about 0.2 %. From the line-chart we can see that the sample mass has no clear tendency to increase or to decrease during 98 hours period. It could be said, that the mass changes are mainly due to the moisture changes in the atmosphere.

It can be concluded, that keeping samples in the formaldehyde liquid does not affect their mass. It could mean that incus bones are more cortical than trabecular.

2.3. EVALUATION OF INCUS MICROSTRUCTURE

To evaluate the volume and microstructure of prepared samples μCTomography analysis was made.

To identify and evaluate the level of bone porosity, bone segmentation also to identify Incus bone type – cortical or trabecular tomography test was used. The μCTomography analysis was made for all four samples.

Before tomography test each sample was glued to the plastic rod which works as a support during scanning. Also, a small aluminium particle was glued to this support to scale the Hounsfield number. The X-ray measurements were performed using "nanotom180N" device produced by GE Sensing & Inspection Technologies phoenix X-ray Gmbh. During the measurement the tungsten target was used. The working parameters of X-ray tube were V=60kV and I=310μA. 1500 projections were taken with an exposure time of 500 milliseconds with 4 integrations for each exposition. The total time of measurement was around 60 min. The reconstruction of measured objects was done with the aid of proprietary GE software datosX ver. 2.1.0 with use of Feldkamp algorithm for cone beam X-ray CT (18). To get the most accurate results 3.5 μm resolution was selected. It means that 1 pixel is equal to 3.5 μm.

The tomography analysis results showed that porosity in incus bone is variable in each part. In the figures below (F*ig.2.12*, *Fig.2.13*, *Fig.2.14* and *Fig.2.15*) is clearly visible that the largest concentration of porosity is in the body. The long and short processes are also porous but the porosity is much lower than in the body.

Also, the tomography results showed that the porosity level of each sample is different. It was noticed after tests that *18ZV* is the most porous sample and the less porous – *1M* specimen.

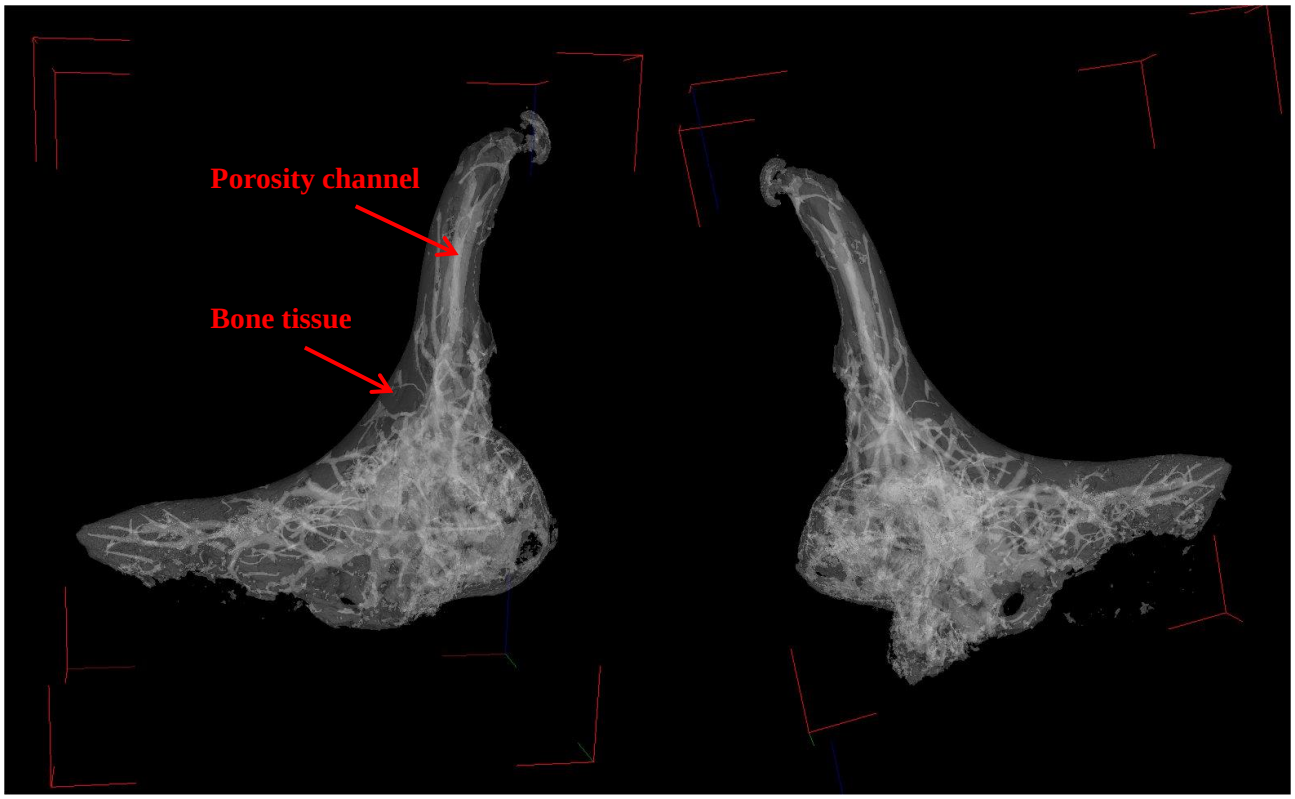

Fig. 2.12 Porosity of sample 1V

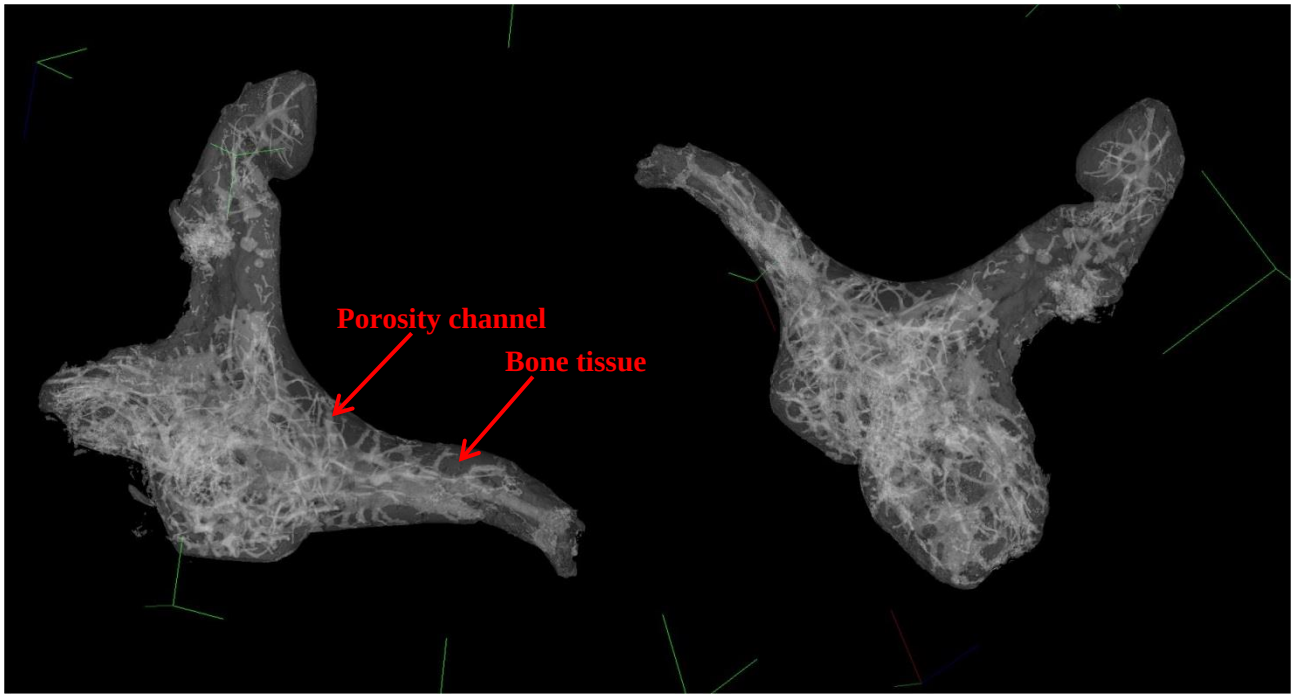

Fig. 2.13 Porosity of sample 18ZV

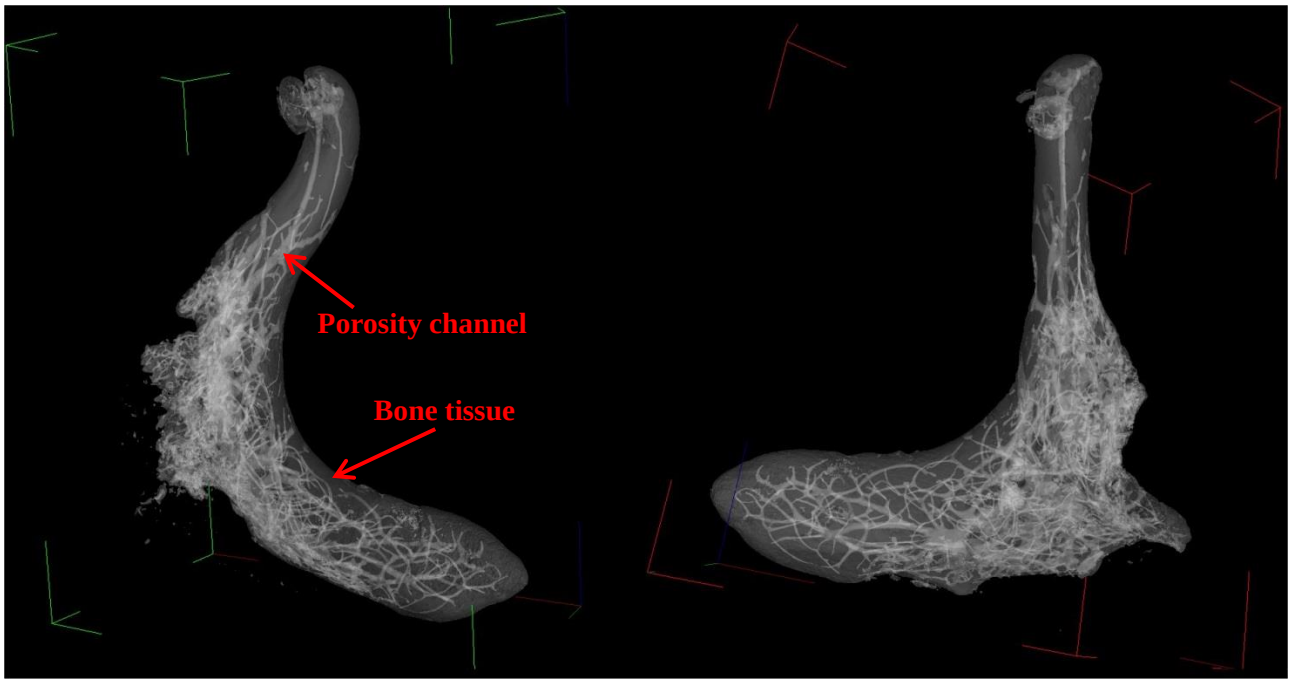

Fig. 2.14 Porosity of sample 1VS

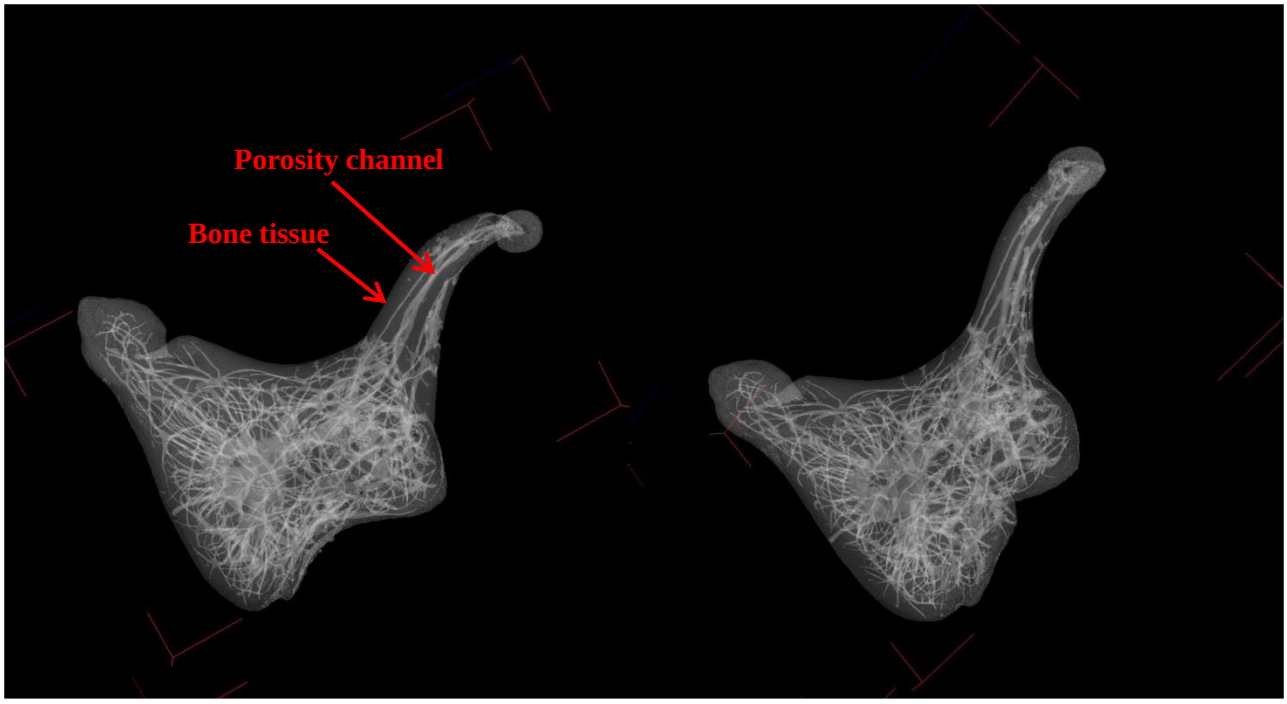

Fig. 2.15 Porosity of sample 1M

After scanning, from the obtained results, using image processing software Fiji®, the volume of each sample was calculated.

Firstly, from all scanned slides were eliminated slides including aluminium particle and support (Fig. 2.16). After, binaries data was prepared consisting only of white and black pixels (Fig. 2.17).

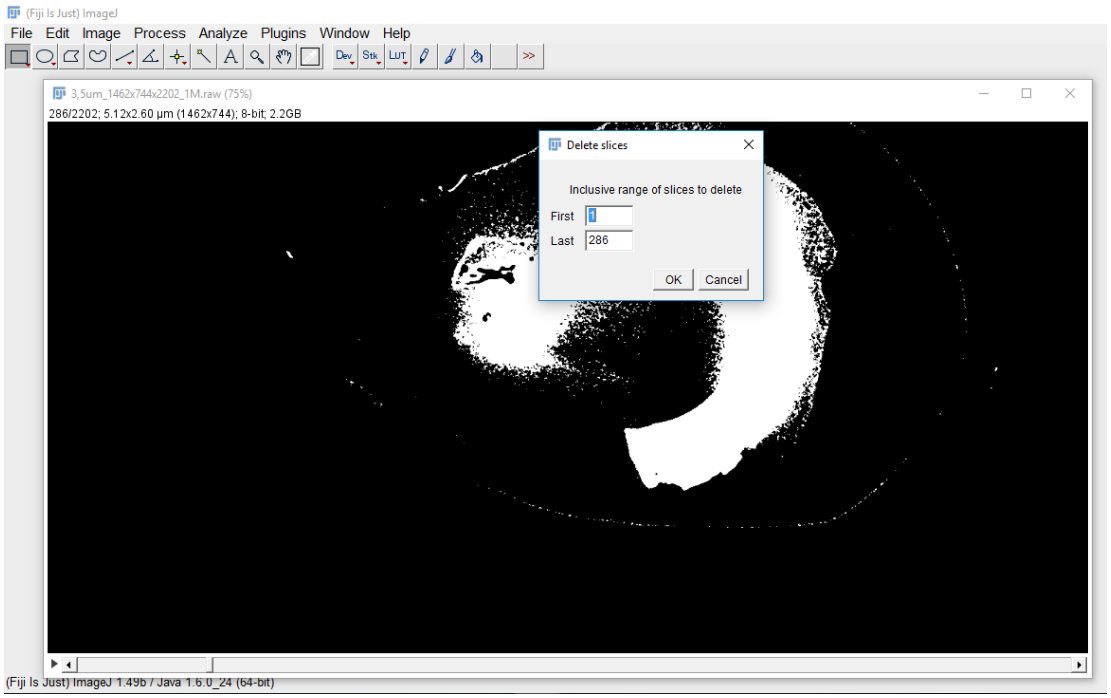

Fig. 2.16 Elimination of slides with aluminium particle

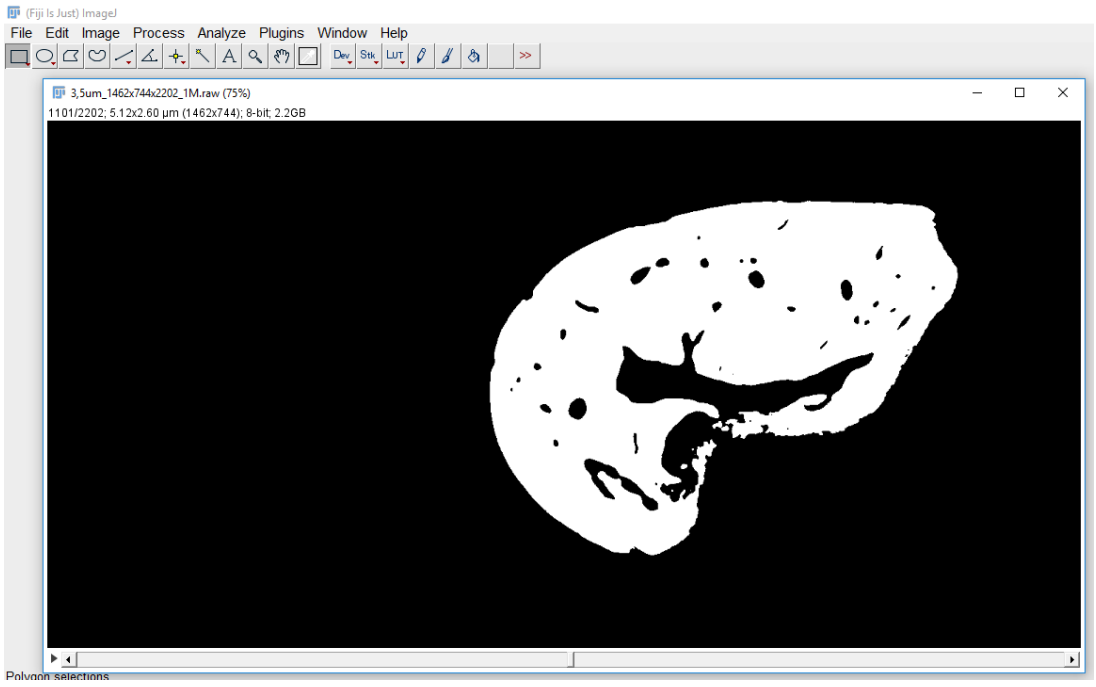

Fig. 2.17 Prepared binaries data

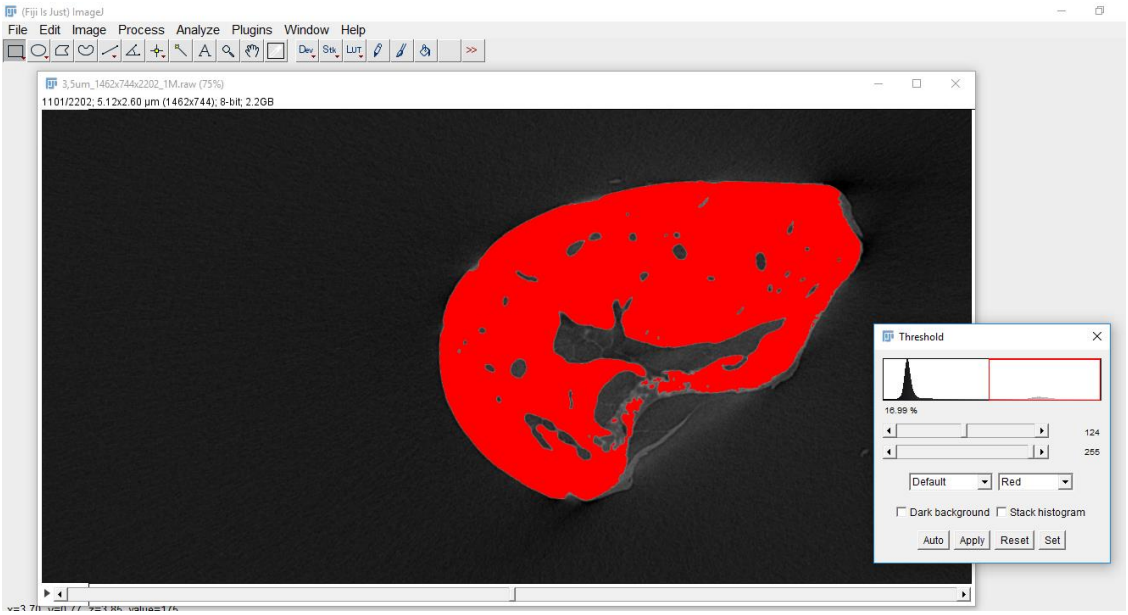

Fig. 2.18 Selection of threshold value

Finally, set threshold values (Fig. 2.18) where set enabling the calculation of volumes of samples. The obtained volume values are presented in *Table 2.6*.

Table 2.6 Volume values of each sample

Sample	**Bone volume, mm^3**	**Mass, g**	**Density, g/cm^3**
1V	15.553	0.01333	0.857
18ZV	13.364	0.01526	1.142
1VS	9.796	0.01580	1.613
1M (without pores)	14.163	0.02881	2.034
1M (with pores)	13.240	0.02881	2.176

For sample *1M* volume was calculated twice: firstly, using scan results as for the others samples, and later for the same model but with manually eliminated porosity. These calculated volume results will be compared with the finite element model volume value.

Knowing, from the measurements presented above the mass of each sample, was performed density (ρ) calculations using formula [1]:

$$\rho = \frac{m}{V} \qquad [1]$$

here:

m – sample mass

V – bone volume.

The results of density calculations are presented in *Table 3.3.1*. As it can be seen, density of samples used for analysis varies in range of 0.857 g/cm^3 (*1V* sample) to 2.176 g/cm^3 (*1M* sample). These apparent density variations show that the microstructure of all four samples is not the same.

It can be concluded, that thanks to the tomography analysis results it was identified complex microstructure of all samples and calculated their volumes and densities. It was founded, that the microstructure of all four samples is damaged and alternated. These microstructure changes decrease the apparent density of the bone.

Various experimental methods can be used to identify the mechanical properties of materials or tissues. The classical mechanical tests such as traction, compression or twisting are frequently used to characterize the properties of materials such as metals or polymers. However, they require the sufficient amount of matter to machine the standard samples. Moreover, they belong to the so-called destructive tests. Recently, nano-indentation has been recognized as a powerful method to estimate local values of Young's modulus of the materials (19). As the classical tests mentioned above, this method leads to a local deterioration of the tested material. On the other hand, ultrasonic methods based on the measurement of sound waves' celerity provide convenient way to characterize the elastic properties of materials and tissues in non-destructive manner. Indeed, the size of the ossicles is too small to use the classical ultrasonic apparatus. Consequently, it was decided to extract the average bone properties by invers method based on the eigenvalues measurement and calculation. To this end the finite element model of *1M* sample was built.

2.4. FREQUENCY EXPERIMENT

To find real value of Incus bone Young's Modulus was decided to make a frequency analysis using piezoelectric system.

F*igure 2.19* shows the place and equipment of experiment. For this analysis was used OPTIKA® TC B5 camera with resolution of 5 Mpixels. Also, was used TOE7404 function generator with frequency range from 0.5 Hz to 5 MHz. Commercial piezo actuator which the precise properties of are unknown. A laptop computer was used to monitor motions of sample.

Fig. 2.19 Frequency experiment

Firstly, the *1M* and *1VS* samples were glued in the centre of the piezoelectric plate (F*ig. 2.20*). As a fixation point was chosen malleus-joint surface. Samples were left completely to dry the glue for a few minutes. After, using function generator manually, the vibration frequency value was increased slowly from 0 to 30 000 Hz to follow body motions.

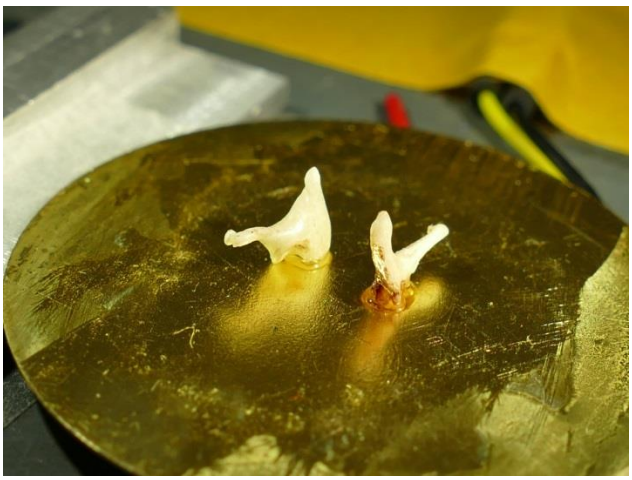

Fig. 2.20 Samples glued on piezoelectric plate

To better to see the body motions and to easily identify frequency range for each mode, camera was zoomed only to the end of long process (F*ig. 2.21*). The registered frequency values are summarised in *Table 2.7*.

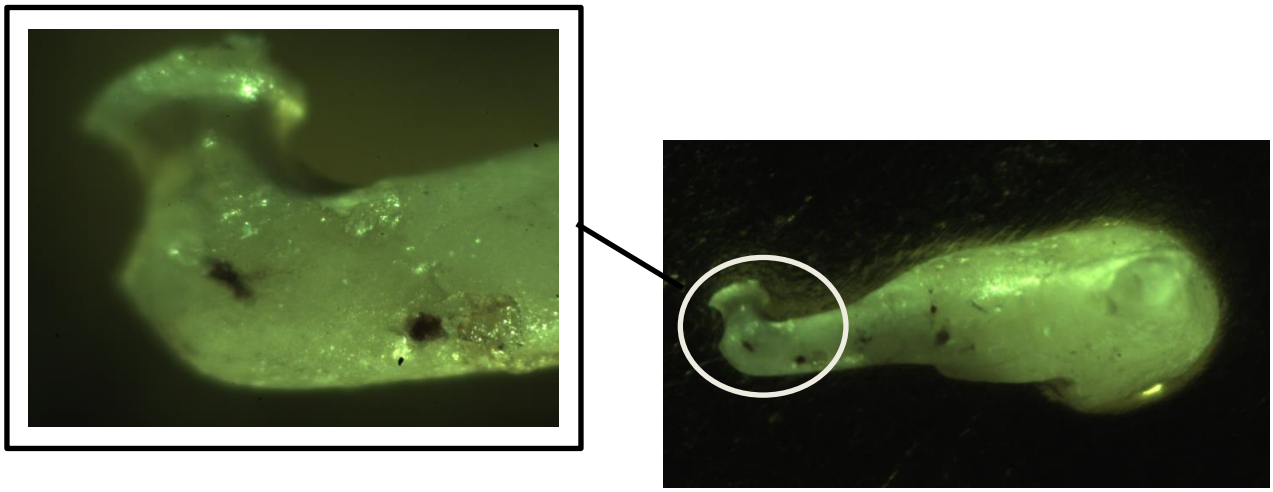

Fig. 2.21 Zoomed long process of *1M* sample

Table 2.7 Registered frequency values

***1VS* Sample**	***1M* Sample**
18.93 kHz	14.18 kHz
19.96 kHz	20.67 kHz
38.81 kHz	30.00 kHz

As it could be seen from the table above, we obtained only three eigenvalues for each sample. The main reason is because that the piezoelectric plate which we used for this analysis was not powerful enough. Also, it is important to mention, that all results was registered only from the view inspection and only in one direction. It means that these values are just approximate.

3. NUMERICAL STUDY OF INCUS

3.1. COMPOSITION OF FINITE ELEMENT MODEL OF INCUS

After the visual exams was decided to simulate the dynamic behaviour of *1M* sample. This sample was chosen because it has the best quality and is closest to the healthy incus bone. It was decided to create two different three-dimensional (3D) models: one as original damaged *1M* sample and other – as non-inflammatory ("healthy") bone.

Using the tomography analysis results was created three-dimensional surface bone model. In *Figure 3.1* can be seen that converting data to *.stl* file causes apparition of numerical artefacts on model such as superimposed triangles and missing parts of surfaces.

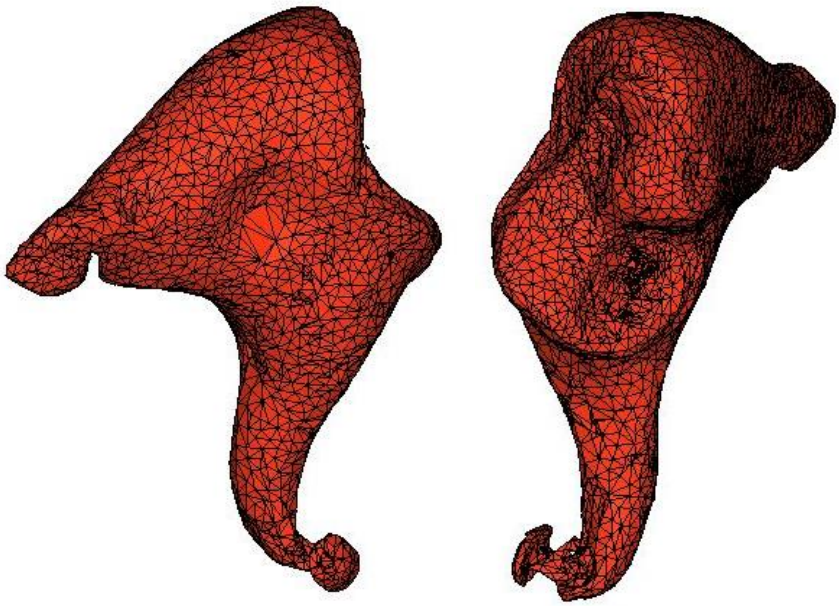

Fig.3.1 Incus bone three-dimensional surface model

Figure 3.2 shows the most affected part of this bone. As can be seen the long process bone tissue is significantly damaged.

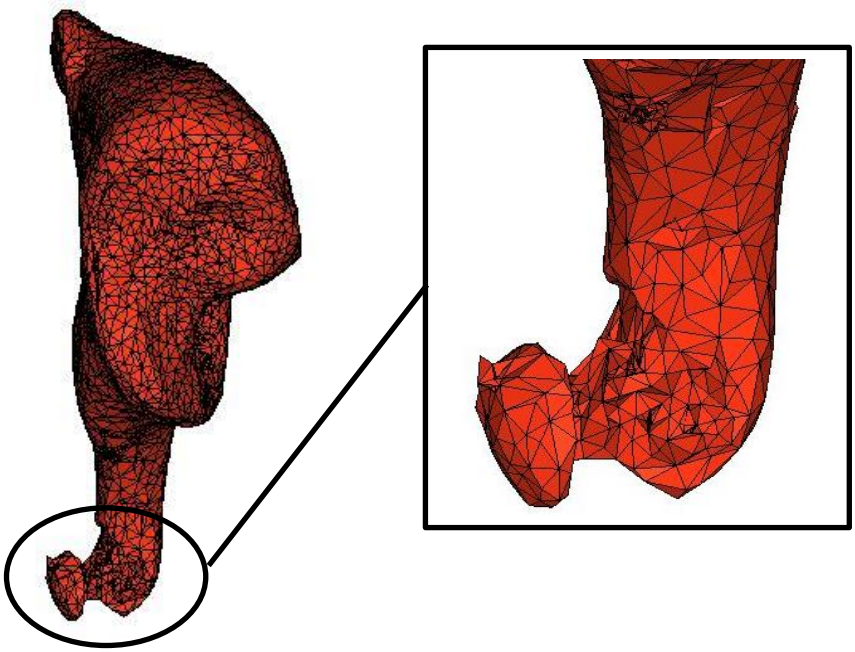

Fig.3.2 Damaged long process tissue

Altair HyperMesh® v 11.0 Software was used to close all surface holes and to make the model smooth. The cleaned and repaired 3D bone model is shown in F*igure 3.3*.

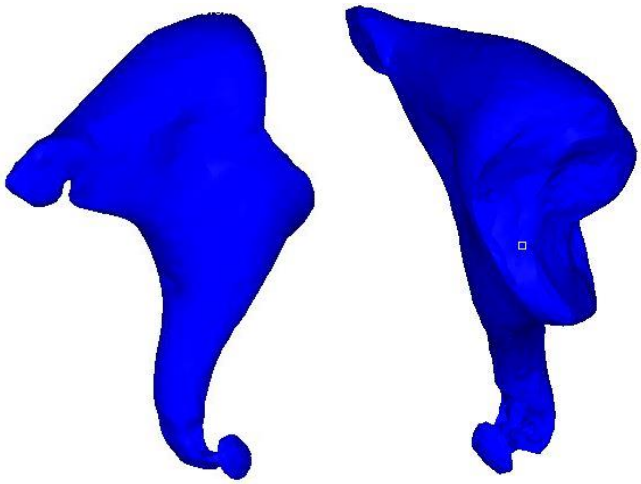

Fig.3.3 Smoothed and repaired 3D bone model

Also, using the same *.stl* file was created non-inflammatory ("Healthy") three-dimensional bone model. It was done by closing surface holes, fixing groove in a short process, repairing damages in long process, and smoothing the whole external surface of the sample. Three different views of "healthy" bone are shown in F*igure 3.4*.

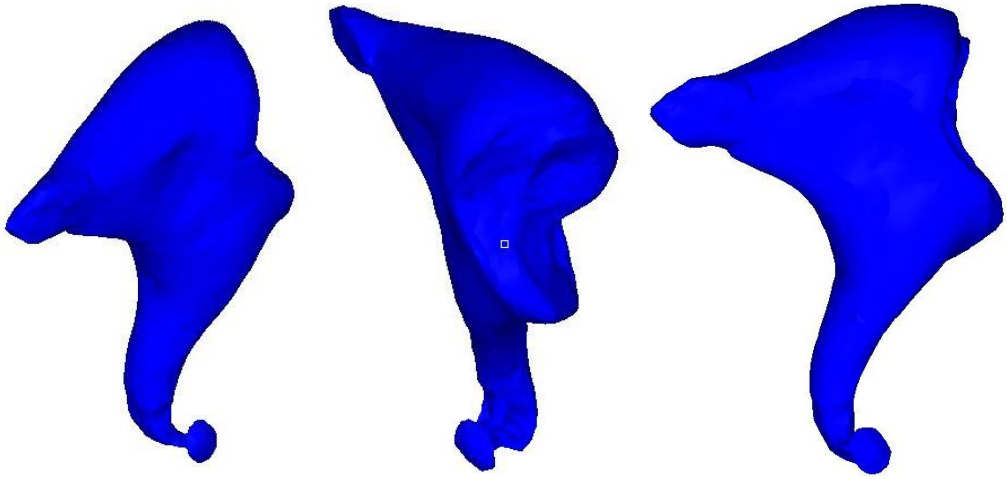

Fig.3.4 Non-inflammatory incus bone 3D model

For both surface models, 2D meshes were firstly created and in the second step 3D meshes were generated (F*ig. 3.5*). For 2D triangular meshing a mean element size was set to 0.06 mm. The 3D meshing was based on 2D ones and led to 102 915 elements for original *1M* sample, and 106 213 elements for "Healthy" one. The grids obtained are illustrated in *Fig. 3.5*.

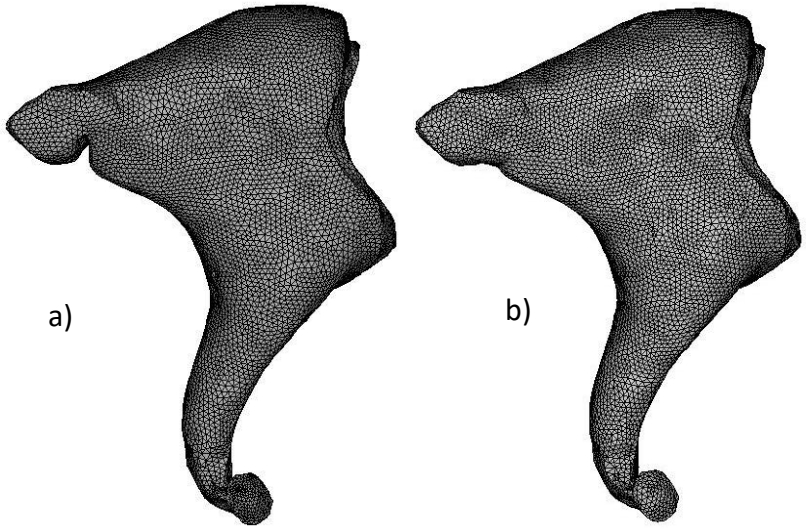

Fig. 3.5 Incus bone 3D mesh: a) Original *1M* sample; b) non-inflammatory bone

To verify the convergence of performed results two types of tetrahedral elements were used. For both models, by changed element class, linear and quadratic versions were prepared. That means that for in the case of linear element type "Quad (4)" class was chosen which consist of

elements with 4 nodes (F*ig.3.6 a)*). For quadratic element type the class was changed to "Tetra (10)" class for which each element is defined by 10 nodes (*Fig.3.6 b)*).

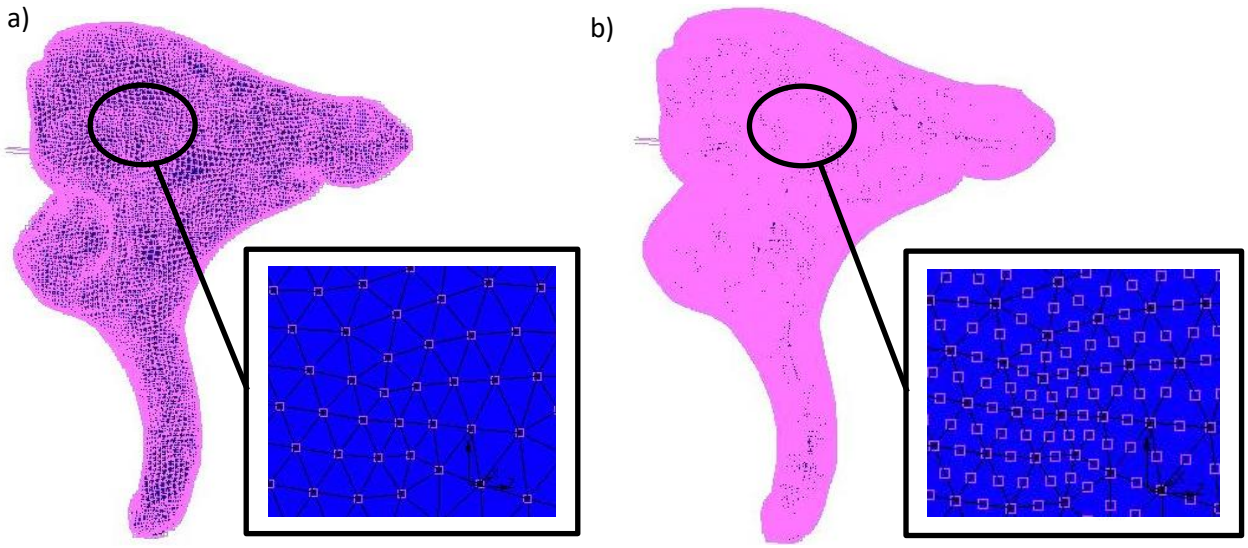

Fig.3.6 3D model: a) linear (4 nodes) element type; b) quadratic (10 nodes) element type

Finally, 4 different models – two with linear type of elements (one original model and one "healthy") and two with quadratic type of elements (one original model and one "healthy") – for dynamic behaviour calculations were prepared. In the *Table 3.1* is presented how many nodes and elements on all occasions were created.

Table 3.1 Number of elements and nodes for each model

Model name	**Number of elements**	**Nodes**	
		Linear (4 nodes) el. type	**Quadratic (10 nodes) el. type**
Original *1M* sample	102 915	22 311	157 226
„Healthy"	106 213	22 935	161 909

When the meshes were created, both 3D models were exported to MSC Marc Mentat® v 2013.1.0 Software. Firstly, for both 3D mesh models, the elastic, linear and isotropic material was associated. The material mechanical properties were chosen with reference to literature (20). We have chosen the value of 1.41 x 10^{10} (N/m^2) for its Young's Modulus and 0.28 as the Poisson's ratio.

As we found in literature (1) and (16), but also as a results of performed tomography analysis, the porosity or internal architecture of bone is not homogeneous and differs from part to part of the bone. Consequently, the density of the incus is not the same in the different parts also. It

means that the bone has different mechanical properties in every part. For this reason, as can be seen in *Fig. 3.7*, both models were divided in three parts – body (in pink), short process (SP – in yellow) and long process (LP – in red).

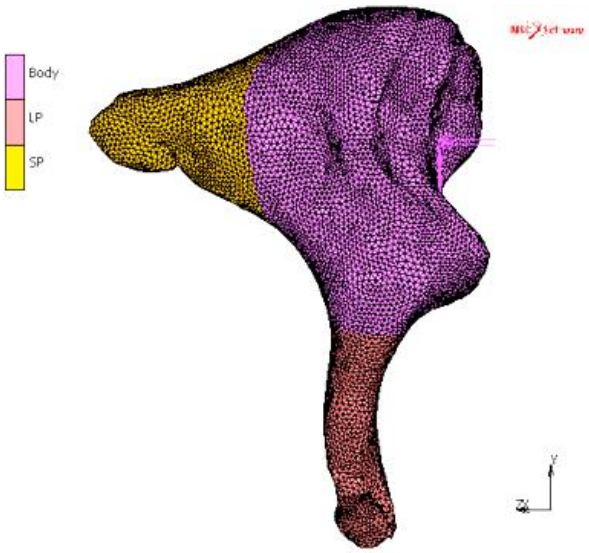

Fig.3.7 *1M* sample 3D mesh model divided in three sections: body, long process (LP) and short process (SP)

To estimate the natural frequencies of the sample, the boundary conditions should be chosen to eliminate the rigid body motion with minimal constraining of the structure.

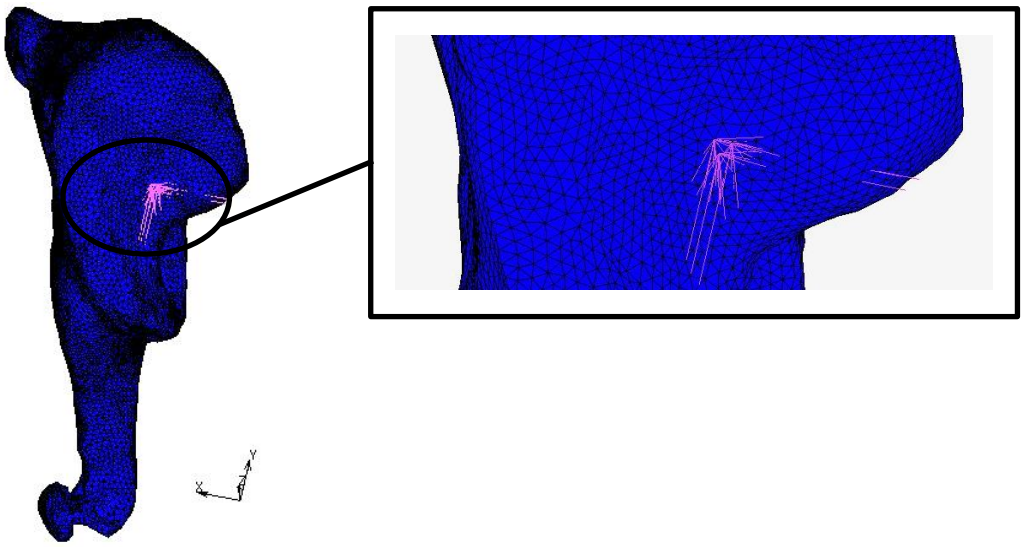

Fig.3.8 Finite element model with boundary conditions

Consequently, it was decided for both models to fix 3 neighbouring nodes in X, Y, Z directions on malleus-joint surface (Fig. 3.8). To create the same boundary conditions for both models the fixed nodes were selected, as much as it was possible in the same place.

3.2. CONVERGENCE ANALYSIS

As a first verification, the volumes of both original and "healthy" models were calculated using the MSC Marc® Software. The results showed that for original *1M* sample model the volume is equal to 14.220 mm^3 and for "healthy" model V = 14.295 mm^3. To compare these results with the results from tomography analysis (where *1M* with pores V = 13.240 mm^3) can be seen that volume value for *1M* 3D model is bigger than calculated with Fiji® Software. Comparing the same finite elements model volume value with *1M* sample without porosity (V = 14.163 mm^3) it was noticed, that the difference is only 0.132 mm4 i.e. less than 0.9 %. Because the volume differences between finite elements model and *1M*-sample without pores is very small, it could mean, that created 3D model of the original *1M*-sample is sufficiently precise.

For all calculations was used MSC Marc® Software. To verify the reliability and the convergence of obtained results, the calculations were repeated five times for each bone geometry of *1M*-sample. Indeed, MSC Marc® provides five types of tetrahedral elements – two linear and three quadratic ones. In the case of linear tetrahedron, it proposes the classical technology (element type n° 134) and Hermann formulation (element type n° 157). For the quadratic elements, there is a choice to choose among the classical technology (element type n° 127), the Hermann formulation (element type n° 130) and "Assumed strain" (element type n° 184). Ten eigenvalues were extracted for each case.

The results from linear element type dynamic calculations are presented in *Table 3.2* those corresponding to the quadratic element type dynamic calculations are gathered in *Table 3.3*.

In all cases three first eigenvalues correspond to the rigid body rotations around the fixed nodes. They are not analysed below. Generally, was observed that the eigenvalues of the "healthy" model are lower than those of the initial or infected bone. This is because "healthy" model has more bone tissue in the long process.

However, exception is made for the modes nine and ten. As it can be seen in Appendix 1, this is due to the fact that the corresponding eigenvectors are different for both bones.

For the Young's modulus chosen and without taking into account the sample porosity, all significant eigenfrequencies are higher than 20 kHz, the threshold frequency of the human ear. Also, significant differences were found between classical and Hermann formulations. For both models, the frequencies are higher in the case of 134-element type than for Hermann formulation.

For instance, this difference is of about 1.5 % in the case of mode 4 of initial geometry. This discrepancy shows that, in spite of relatively small element size (0.06 mm), the grid with linear classical elements is too stiff.

Table 3.2 Model with linear element type dynamic behaviour

Linear (4 nodes) el. type	**Original *1M* sample**	**"Healthy" bone model**
Full Integration (134)	Inc / Time / Freq 0 / 0 / 0 0:1 / 0 / 796.648 0:2 / 0 / 1424.54 0:3 / 0 / 1945.25 0:4 / 0 / 38346.2 0:5 / 0 / 46747.4 0:6 / 0 / 57154.3 0:7 / 0 / 62674.4 0:8 / 0 / 64544.9 0:9 / 0 / 77031.8 0:10 / 0 / 100375	Inc / Time / Freq 0 / 0 / 0 0:1 / 0 / 737.513 0:2 / 0 / 955.103 0:3 / 0 / 1550.77 0:4 / 0 / 32911.7 0:5 / 0 / 40615.7 0:6 / 0 / 51008.7 0:7 / 0 / 55431.2 0:8 / 0 / 59160.1 0:9 / 0 / 91974.5 0:10 / 0 / 102902
Full Integration & Herman Formulation (157)	Inc / Time / Freq 0 / 0 / 0 0:1 / 0 / 756.446 0:2 / 0 / 1363.26 0:3 / 0 / 1844.19 0:4 / 0 / 37782.3 0:5 / 0 / 45993.5 0:6 / 0 / 56195.1 0:7 / 0 / 61175.4 0:8 / 0 / 64089.8 0:9 / 0 / 75414 0:10 / 0 / 99652.7	Inc / Time / Freq 0 / 0 / 0 0:1 / 0 / 705.533 0:2 / 0 / 919.265 0:3 / 0 / 1467.71 0:4 / 0 / 32385.3 0:5 / 0 / 39976.9 0:6 / 0 / 50124.8 0:7 / 0 / 53853.8 0:8 / 0 / 58898.3 0:9 / 0 / 91081 0:10 / 0 / 102248

The situation is similar for the quadratic grids (see *Table 3.3*). Main difference between these two tables concerns the significant decrease of eigenvalues obtained with quadratic elements. Indeed, for instance in the case of mode 4 and classical formulations, the eigenvalues are of 38.346 kHz and 28.427 kHz, respectively for linear and quadratic elements. It represents nearly 35% of difference. The softest response of the model was obtained for full integration & "assumed strain" technology (element n° 184). However, the difference between the results of classical and assumed strain formulations is less than 1.6%. Consequently, the all remaining calculations and invers method were done using quadratic elements with "assumed strain" technology.

Table 3.3 Model with quadratic element type dynamic behaviour

Quadratic (10 nodes) el. type	**Original *1M* sample**	**"Healthy" bone model**
Full Integration (127)	Inc / Time / Freq 0 / 0 / 0 0:1 / 0 / 447.501 0:2 / 0 / 793.761 0:3 / 0 / 1146.42 0:4 / 0 / 28427.1 0:5 / 0 / 35738.9 0:6 / 0 / 45603.3 0:7 / 0 / 48430.4 0:8 / 0 / 59624 0:9 / 0 / 66728.7 0:10 / 0 / 93338.3	Inc / Time / Freq 0 / 0 / 0 0:1 / 0 / 404.858 0:2 / 0 / 556.33 0:3 / 0 / 912.426 0:4 / 0 / 24059 0:5 / 0 / 30925.3 0:6 / 0 / 39992.3 0:7 / 0 / 44779.5 0:8 / 0 / 57535.8 0:9 / 0 / 84750.1 0:10 / 0 / 98515.3
Full Integration & Herman Formulation (130)	Inc / Time / Freq 0 / 0 / 0 0:1 / 0 / 436.386 0:2 / 0 / 772.635 0:3 / 0 / 1091.58 0:4 / 0 / 27735.7 0:5 / 0 / 34708.7 0:6 / 0 / 44124.6 0:7 / 0 / 47982 0:8 / 0 / 59521.2 0:9 / 0 / 66621.4 0:10 / 0 / 93255	Inc / Time / Freq 0 / 0 / 0 0:1 / 0 / 397.173 0:2 / 0 / 545.053 0:3 / 0 / 864.109 0:4 / 0 / 23674 0:5 / 0 / 30029 0:6 / 0 / 38606.4 0:7 / 0 / 44528.8 0:8 / 0 / 57506.5 0:9 / 0 / 84702 0:10 / 0 / 98463.9
Full Integration & Assumed Strain (184)	Inc / Time / Freq 0 / 0 / 0 0:1 / 0 / 435.069 0:2 / 0 / 771.88 0:3 / 0 / 1116.9 0:4 / 0 / 27882.6 0:5 / 0 / 35153.5 0:6 / 0 / 44818.7 0:7 / 0 / 48153.4 0:8 / 0 / 59350.6 0:9 / 0 / 66526.4 0:10 / 0 / 93116.4	Inc / Time / Freq 0 / 0 / 0 0:1 / 0 / 393.182 0:2 / 0 / 540.687 0:3 / 0 / 888.493 0:4 / 0 / 23595.3 0:5 / 0 / 30421.2 0:6 / 0 / 39282 0:7 / 0 / 44624.6 0:8 / 0 / 57498.8 0:9 / 0 / 84528.1 0:10 / 0 / 98408.5

The last test concerns the analysis of the influence of Poisons ratio or material compressibility on the eigenvalues. The simulations were done with three values of the Poison's ratio, namely 0.28 to 0.30 and 0.40. All results are presented in *Table 3.4* and plotted in *Figure 3.9*. From the results could be said that increasing Poison's ratio results in increase of eigenfrequencies. However, it could be concluded that because differences between results with different Poisson's ratio is slight, the initial value of this constant is retained for the invers method of elastic modulus identification.

Table 3.4 *1M*-sample frequencies with different Poison's Ratio

Modes	Frequencies (Hz), when Poison's ratio:		
	0.28	**0.30**	**0.40**
1	435.069	436.093	447.693
2	771.88	773.168	792.621
3	1116.9	1115.74	1126.45
4	27882.6	27934.9	28575.8
5	35153.5	35159.4	35568.2
6	44818.7	44786.6	45131.7
7	48153.4	48132.9	48195.5
8	59350.6	59415.3	59818.9
9	66526.4	66522.2	66592
10	93116.4	92821.3	91484.4

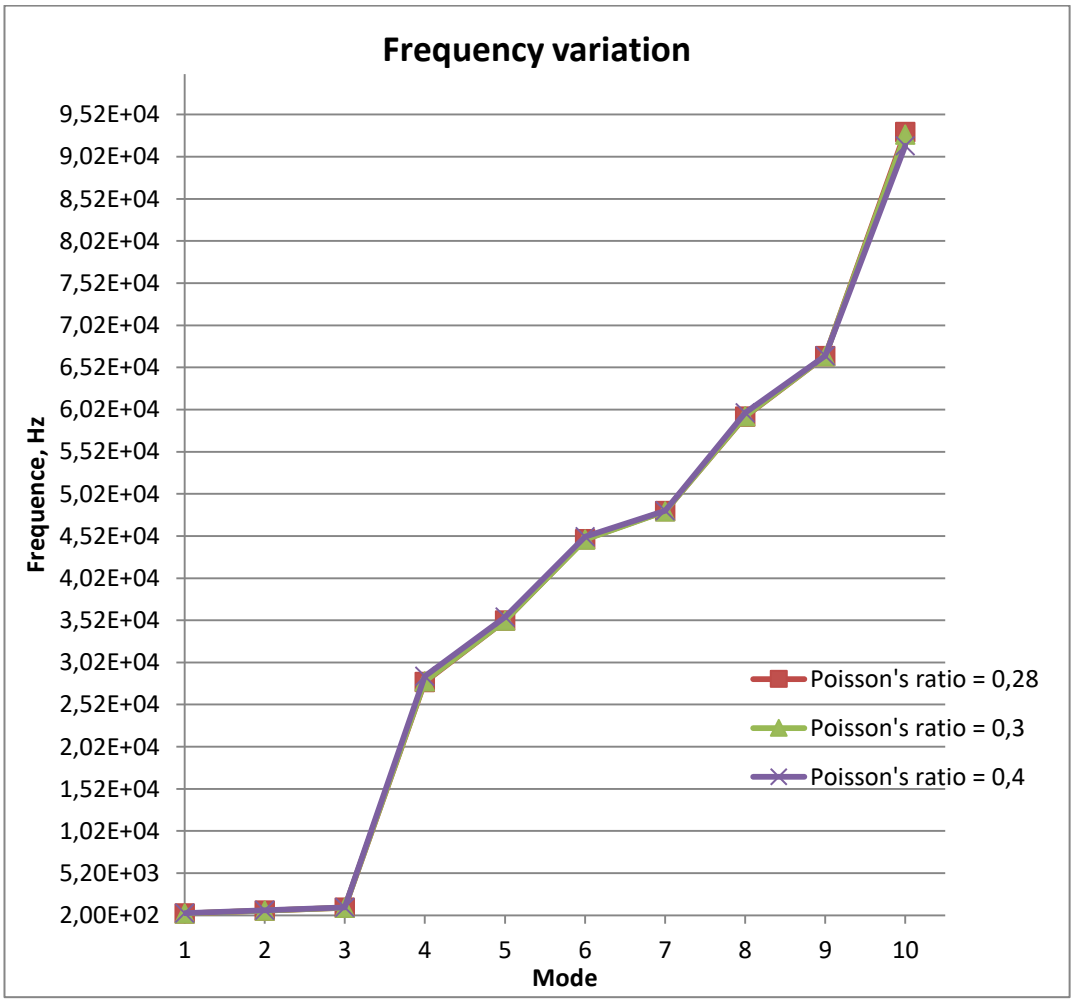

Fig.3.9 *1M*-sample frequencies with different Poison's Ratio

3.3. DISPLACEMENT ANALYSIS

To better understand body behaviour during vibrations, displacements fields were calculated. All displacement maps are shown in Appendix II.

In the figures of Appendix II. I are shown displacements for finite element models with linear type of elements and in the Appendix II.II – displacements for models with quadratic type of elements. From the figures, can be seen, that in 1 – 3 modes original *1M* sample and "healthy" bone perform body rigid rotations. Comparing 4th mode of both models can be seen that long process perform bending motion around X-axis. In the *Figure 3.10* of 5th mode shows that the long process also performs motion around X-axis, but in the opposite direction than in the 4th mode. The colour map shows that the highest displacement values were obtained in body and in the short process parts.

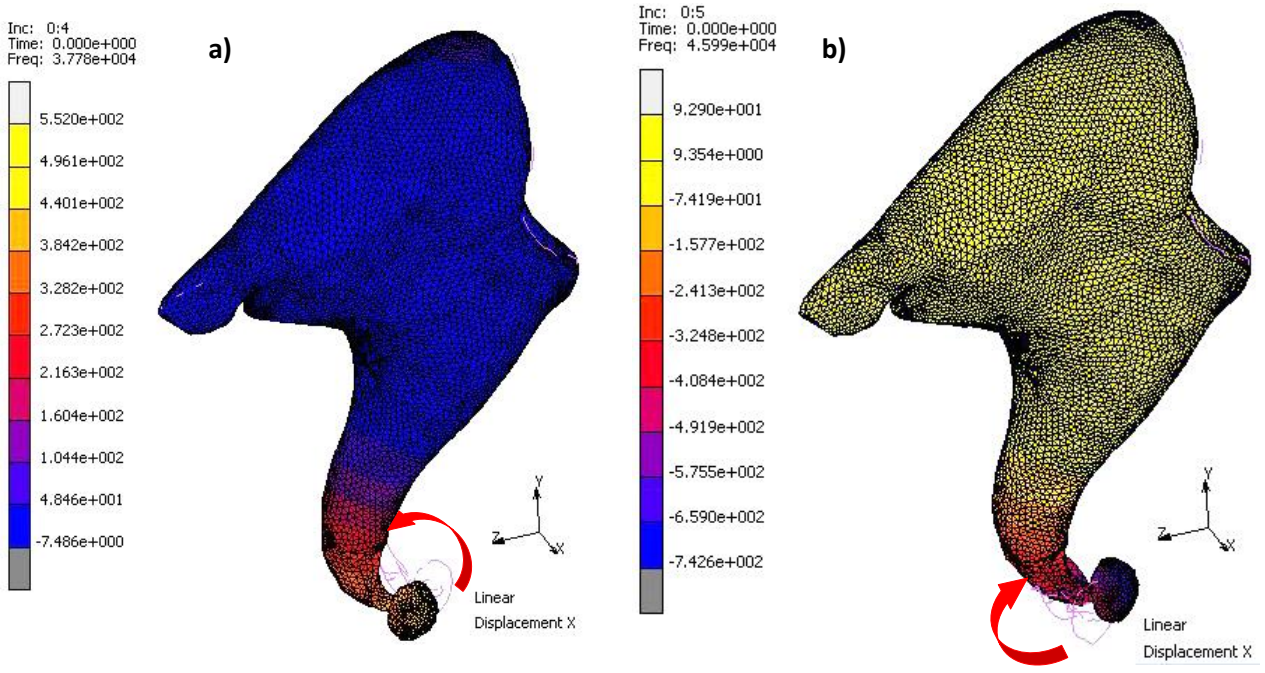

Fig.3.10 Long process motions around X-axis: a) 4th mode; b) 5th mode

In the 6th mode models perform bending motions along Z-axis. Also in this mode for models with quadratic type of elements can be seen short process motions around Y-axis. In the 7th mode for models with linear type of elements, are performed motions around Y-axis, but in the same mode, for models with quadratic type of elements is showed, that long process is moving around X-axis, but in the opposite directions for "healthy" and for original *1M* models.

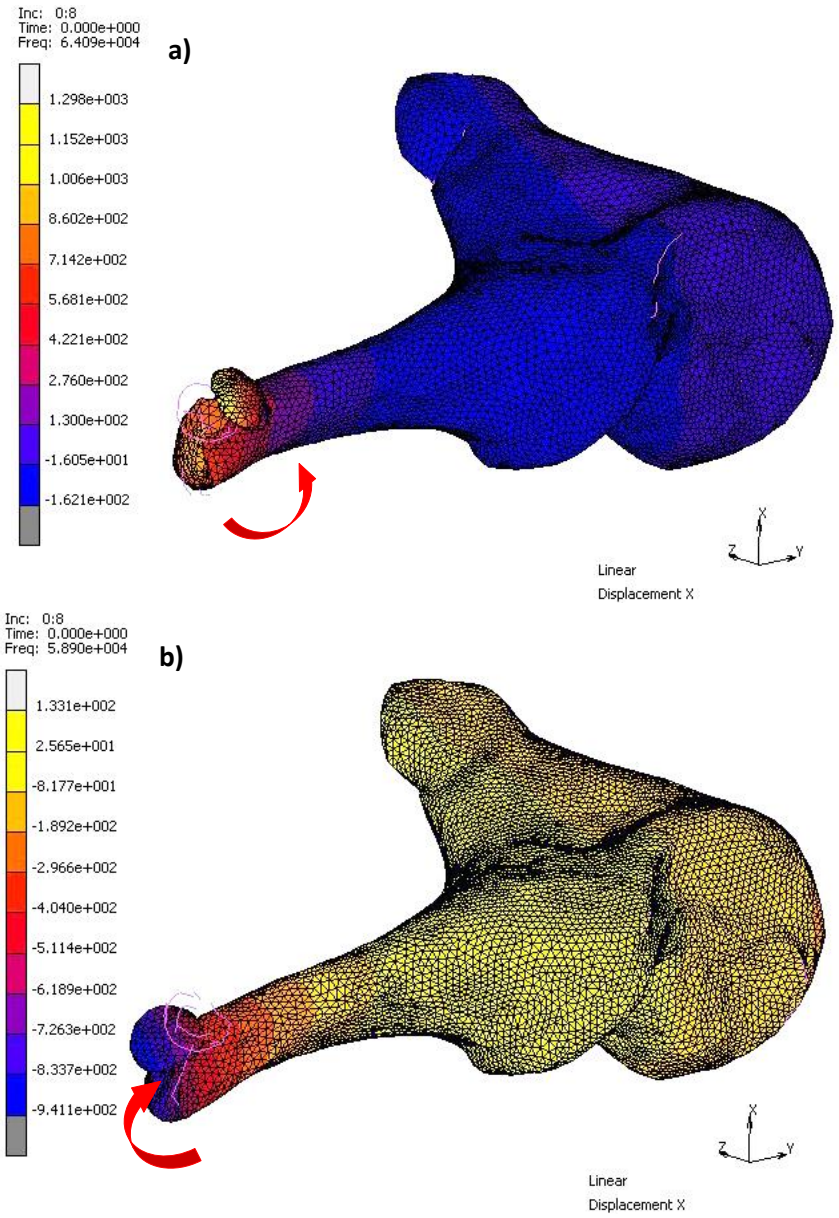

Fig.3.11 Long process motions around Z-axis: a) Original 1M sample; b) "Healthy" bone model

In the *Figure 3.11* of 8th mode long process of the models performed motions around Z-axis, but as it is shown in the figures, in the opposite directions for the original *1M* and the "healthy" model. In the 8, 9 and 10 modes motion direction differences between original and "healthy" models are represented. These differences could perform because the "healthy" bone model is stiffer in its long process.

To conclude, it could be said, that from the frequency calculations results can be taken into account only from the 4th to 7th modes. Because first three values perform rigid body rotations, and the last three – have the different motion directions because model thickness differences in long process.

3.4. YOUNG'S MODULUS IDENTIFICATION

To identify sample material properties was decided to identify Young's modulus using results from vibration test.

1M-sample model with quadratic element type (element type n° 184) was used for Young's modulus identification. 10 calculations were done, shown in *Table 3.5*, by changing these properties to fit the experimentally determined eigenfrequencies.

Table 3.5 Young's modulus identification

Young's Modulus, N/m^2	**Frequency, Hz**	**Young's Modulus, N/m^2**	**Frequency, Hz**
1.41 x 10^{10}	Inc / Time / Freq 0 / 0 / 0 0:1 / 0 / 435.069 0:2 / 0 / 771.88 0:3 / 0 / 1116.9 0:4 / 0 / 27882.6 0:5 / 0 / 35153.5 0:6 / 0 / 44818.7 0:7 / 0 / 48153.4 0:8 / 0 / 59350.6 0:9 / 0 / 66526.4 0:10 / 0 / 93116.4	1.3 x 10^{10}	Inc / Time / Freq 0 / 0 / 0 0:1 / 0 / 418.425 0:2 / 0 / 742.351 0:3 / 0 / 1074.17 0:4 / 0 / 26815.9 0:5 / 0 / 33808.7 0:6 / 0 / 43104.1 0:7 / 0 / 46311.3 0:8 / 0 / 57080.1 0:9 / 0 / 63981.4 0:10 / 0 / 89554.2
1.1 x 10^{10}	Inc / Time / Freq 0 / 0 / 0 0:1 / 0 / 384.895 0:2 / 0 / 682.864 0:3 / 0 / 988.093 0:4 / 0 / 24667 0:5 / 0 / 31099.5 0:6 / 0 / 39650 0:7 / 0 / 42600.2 0:8 / 0 / 52506.1 0:9 / 0 / 58854.3 0:10 / 0 / 82377.8	1 x 10^{10}	Inc / Time / Freq 0 / 0 / 0 0:1 / 0 / 366.983 0:2 / 0 / 651.085 0:3 / 0 / 942.11 0:4 / 0 / 23519.1 0:5 / 0 / 29652.2 0:6 / 0 / 37804.8 0:7 / 0 / 40617.7 0:8 / 0 / 50062.6 0:9 / 0 / 56115.4 0:10 / 0 / 78544.2
9 x 10^9	Inc / Time / Freq 0 / 0 / 0 0:1 / 0 / 348.151 0:2 / 0 / 617.674 0:3 / 0 / 893.764 0:4 / 0 / 22312.2 0:5 / 0 / 28130.5 0:6 / 0 / 35864.8 0:7 / 0 / 38533.3 0:8 / 0 / 47493.5 0:9 / 0 / 53235.7 0:10 / 0 / 74513.6	7 x 10^9	Inc / Time / Freq 0 / 0 / 0 0:1 / 0 / 307.04 0:2 / 0 / 544.737 0:3 / 0 / 788.225 0:4 / 0 / 19677.5 0:5 / 0 / 24808.8 0:6 / 0 / 31629.8 0:7 / 0 / 33983.2 0:8 / 0 / 41885.4 0:9 / 0 / 46949.5 0:10 / 0 / 65714.8

6×10^9

Inc	Time	Freq
0	0	0
0:1	0	284.264
0:2	0	504.328
0:3	0	729.755
0:4	0	18217.8
0:5	0	22968.5
0:6	0	29283.5
0:7	0	31462.3
0:8	0	38778.3
0:9	0	43466.8
0:10	0	60840.1

5.5×10^9

Inc	Time	Freq
0	0	0
0:1	0	272.162
0:2	0	482.858
0:3	0	698.687
0:4	0	17442.2
0:5	0	21990.6
0:6	0	28036.8
0:7	0	30122.9
0:8	0	37127.4
0:9	0	41616.3
0:10	0	58249.9

5×10^9

Inc	Time	Freq
0	0	0
0:1	0	259.496
0:2	0	460.387
0:3	0	666.172
0:4	0	16630.5
0:5	0	20967.3
0:6	0	26732
0:7	0	28721
0:8	0	35399.6
0:9	0	39679.6
0:10	0	55539.1

4.5×10^9

Inc	Time	Freq
0	0	0
0:1	0	246.18
0:2	0	436.761
0:3	0	631.986
0:4	0	15777.1
0:5	0	19891.3
0:6	0	25360.2
0:7	0	27247.2
0:8	0	33583
0:9	0	37643.4
0:10	0	52689

The resulting eigenfrequencies showed that the Young's Modulus equal to 4.5×10^9 (N/m^2) provided the response closest to the experimentally obtain eigenvalues. Also, it should be mentioned that calculations were made using bone model in which porosity is not included.

We also tried to take into account the sample inhomogeneity. Basing on literature [(1), (16)] and (21) we have set the density of the long process of *1M*-sample to 5.08×10^3 kg/m^3 .The simulations were repeated for two values of Young' modulus, namely 4.5×10^9 and 6×10^9 N/m^2. The obtained results are presented in *Table 3.6.*

Table 3.6 Frequency, when the density of long process is 5.08×10^3 kg/m^3

Young's Modulus, N/m^2	**4.5×10^9**	**6×10^9**
Results		

Inc	Time	Freq
0	0	0
0:1	0	222.159
0:2	0	409.581
0:3	0	598.154
0:4	0	14857.5
0:5	0	18962.3
0:6	0	22593
0:7	0	23713.4
0:8	0	28215.8
0:9	0	28340.4
0:10	0	36659.8

Inc	Time	Freq
0	0	0
0:1	0	256.527
0:2	0	472.943
0:3	0	690.688
0:4	0	17156
0:5	0	21895.7
0:6	0	26088.1
0:7	0	27381.9
0:8	0	32580.7
0:9	0	32724.7
0:10	0	42331.1

Comparing results from *Table 3.5* with results from *Table 3.6* it was noticed that when the density of *1M*-sample is not homogeneous the frequency values obtained for $E=4.5 \times 10^9$ N/m^2 are lower than experimental ones. Consequently, this enabled us to increase this modulus to $E=6 \times 10^9$ N/m^2 to fit better the experimental values.

CONCLUSIONS

1. In order to identify Incus bone microstructure and mechanical properties, firstly, visual analysis was made for four samples. This inspection allowed to establish the most damaged and the healthiest sample. Also, the mass of all samples was measured and identified that mass varies in range of 0.01333 – 0.02881 g. It was noticed that mass changes appeared because of the ambient humidity variation, but not because of bone water contents.

2. After tomography result analysis it was identified that microstructure and porosity of bone are not homogeneous and differ from part to part of the bone. It could be said, that bone samples used for experiments are more porous than typical cortical bone. Also, it was found that that microstructure of samples used for research is very different because samples density varies in range from 0.857 g/cm^3 to 2.176 g/cm^3.

3. To find real value of the average incus bone Young's Modulus the modal analysis using piezoelectric exciter was performed. Two different incus samples were tested and 3 modes were found in the range of 14.18 kHz - 38.81 kHz.

4. From tomography results 3D Finite Element models were created: real incus and healthy (the infected part was remodelled) one. It was found that, because "healthy" model has more bone tissue in the long process the eigenvalues of the "healthy" model are lower than those of the infected bone. Furthermore, significant differences were found between classical and Hermann formulations of FEM. For both FE models – original 1M-sample and the "healthy" one – the frequencies are 1.6 % higher in the case of 134-element. Also, it was noticed significant decrease of eigenvalues obtained for models with quadratic elements comparing with linear ones – the difference is about 35 %.

5. Poison's ratio influence was tested on the eigenvalues, and it was found that differences between results with various Poisson's ratio are slight, and the initial value of this constant was retained for the invers method of elastic modulus identification.

6. Comparing frequency values obtained from experiment with frequencies calculated by changing Young's Modulus value, it was found that the calculated eigenfrequencies are closest to real value, if the Young's Modulus is equal to 4.5 x 10^9 N/m^2.

RECOMMENDATIONS

The results obtained during this research have to be treated as the first approximation because all calculations were done not taking into account the actual bone porosity. Moreover, on purpose to found out Incus bone mechanical properties, the real density of each bone part has to be identified. Also, to get reliable results, all calculations should be repeated using bone model with porosity. Furthermore, it is important to mention that, to get reliable results for this research more than one computational model should be used.

ACKNOWLEDGEMENTS

Firstly, I would like to thank to prof. Pawel Lipinski from Université de Lorraine, Ecole Nationale d'Ingénieurs de Metz. I am grateful for his help, concern, lessons and the imparted knowledge during all Erasmus+ internship in France from 1st of June to 31st of July.

Also, I would like to thank for dr. Sebastian Wronski from the group of Pr Jacek Tarasiuk of Cracow University of Science and Technology – AGH for his help and advices performing bone microstructure analysis.

Finally, I would like to thank to prof. Rachid Rahouadj from Université de Lorraine, LEMTA for his help accomplishing frequency analysis.

I would like to thank to MD Giedrius Gylys and Kristina Norkaityte of ORL Department, Lithuanian University of Health Sciences for the imparted knowledge about hearing system.

REFERENCES

1. LIU, Houguang, RAO, Zhushi, HUANG, Xinsheng, CHENG, Gang, TIAN, Jiabin, TA, Na, LIU, Houguang, RAO, Zhushi, HUANG, Xinsheng, CHENG, Gang, TIAN, Jiabin and TA, Na. An Incus-Body Driving Type Piezoelectric Middle Ear Implant Design and Evaluation in 3D Computational Model and Temporal Bone, An Incus-Body Driving Type Piezoelectric Middle Ear Implant Design and Evaluation in 3D Computational Model and Temporal Bone. *The Scientific World Journal, The Scientific World Journal*. 18 June 2014. Vol. 2014, 2014, p. e121624. DOI 10.1155/2014/121624, 10.1155/2014/121624.

2. FERRIS, P. and PRENDERGAST, P. J. Middle-ear dynamics before and after ossicular replacement. *Journal of Biomechanics*. gegužės 2000. Vol. 33, no. 5, p. 581–590. DOI 10.1016/S0021-9290(99)00213-4.

3. ALBERA, R., CANALE, A., PIUMETTO, E., LACILLA, M. and DAGNA, F. Ossicular chain lesions in cholesteatoma. *Acta Otorhinolaryngologica Italica*. October 2012. Vol. 32, no. 5, p. 309. PMID: 23326010

4. DUBOEUF, François, BURT-PICHAT, Brigitte, FARLAY, Delphine, SUY, Paul, TRUY, Eric and BOIVIN, Georges. Bone quality and biomechanical function: A lesson from human ossicles. *Bone*. balandžio 2015. Vol. 73, p. 105–110. DOI 10.1016/j.bone.2014.12.009.

5. *Rimvydas Stropus, Kazys Algimantas Tamašauskas, Neringa Paužienė ŽMOGAUS ANATOMIJA'', Kaunas, Vitae Litera, 2005.pdf.*

6. Ear-anatomy.jpg (JPEG paveikslas, dydis: 526 × 440 taškelių). [online]. [Accessed 24 June 2016]. Available from: http://www.biographixmedia.com/human/ear-anatomy.jpg

7. BRUNS, Alan D and RUCKENSTEIN, Michael J. Middle Ear Function: Overview, What is Sound?, External Ear. [online]. 28 April 2016. [Accessed 24 June 2016]. Available from: http://emedicine.medscape.com/article/874456-overview

8. STOESSEL, Alexander, GUNZ, Philipp, DAVID, Romain and SPOOR, Fred. Comparative anatomy of the middle ear ossicles of extant hominids – Introducing a geometric morphometric protocol. *Journal of Human Evolution*. vasario 2016. Vol. 91, p. 1–25. DOI 10.1016/j.jhevol.2015.10.013.

9. KOVINCIC, Nemanja I. and SPASIC, Dragan T. Dynamics of a middle ear with fractional type of dissipation. *Nonlinear Dynamics*. 1 September 2016. Vol. 85, no. 4, p. 2369–2388. DOI 10.1007/s11071-016-2832-z.

10. KAFTAN, Holger, BÖHME, Andrea and MARTIN, Heiner. Parameters for novel incus replacement prostheses. *European Archives of Oto-Rhino-Laryngology*. 1 September 2016. Vol. 273, no. 9, p. 2411–2417. DOI 10.1007/s00405-015-3810-7.

11. Types, Causes and Treatment | Hearing Loss Association of America. [online]. [Accessed 24 June 2016]. Available from: http://www.hearingloss.org/content/types-causes-and-treatment

12. Ar įmanoma pagerinti pablogėjusią klausą? - Ausų, nosies, gerklės ligos - Sveikas Žmogus. [online]. [Accessed 17 June 2016]. Available from: http://www.sveikaszmogus.lt/Ausu_nosies_gerkles_ligos-6896

13. BORGSTEIN, J., GERRITSMA, T. V. and BRUCE, I. A. Erosion of the incus in pediatric posterior tympanic membrane retraction pockets without cholesteatoma. *International Journal of Pediatric Otorhinolaryngology*. rugsėjo 2008. Vol. 72, no. 9, p. 1419–1423. DOI 10.1016/j.ijporl.2008.06.004.

14. PARK, Keehyun, CHOUNG, Yun-Hoon, REE SHIN, You and PYO HONG, Sung. Conductive deafness with normal eardrum: absence of the long process of the incus. *Acta Oto-Laryngologica*. January 2007. Vol. 127, no. 8, p. 816–820. DOI 10.1080/00016480601075449.

15. YUNG, M.w. Retraction of the pars tensa — long-term results of surgical treatment. *Clinical Otolaryngology & Allied Sciences*. rugpjūčio 1997. Vol. 22, no. 4, p. 323–326. DOI 10.1046/j.1365-2273.1997.00018.x.

16. SUN, Q., GAN, R. Z., CHANG, K.-H. and DORMER, K. J. Computer-integrated finite element modeling of human middle ear. *Biomechanics and Modeling in Mechanobiology*. Vol. 1, no. 2, p. 109–122. DOI 10.1007/s10237-002-0014-z.

17. VOLANDRI, G., DI PUCCIO, F., FORTE, P. and CARMIGNANI, C. Biomechanics of the tympanic membrane. *Journal of Biomechanics*. balandžio 2011. Vol. 44, no. 7, p. 1219–1236. DOI 10.1016/j.jbiomech.2010.12.023.

18. *Feldkamp, L. A.; Davis, L. C.; Kress, J.W. 1984. Practical cone-beam algorithm JOSA A, 1(6): 612–619.*

19. OLIVER, W.C. and PHARR, G.M. An improved technique for determining hardness and elastic modulus using load and displacement sensing indentation experiments. *Journal of Materials Research*. June 1992. Vol. 7, no. 6, p. 1564–1583. DOI 10.1557/JMR.1992.1564.

20. ZHANG, Xiangming, GUAN, Xiying, NAKMALI, Don, PALAN, Vikrant, PINEDA, Mario and GAN, Rong Z. Experimental and Modeling Study of Human Tympanic Membrane Motion in the Presence of Middle Ear Liquid. *Journal of the Association for Research in Otolaryngology*. 9 August 2014. Vol. 15, no. 6, p. 867–881. DOI 10.1007/s10162-014-0482-8.

21. LEE, Dooho and AHN, Tae-Soo. Statistical calibration of a finite element model for human middle ear. *Journal of Mechanical Science and Technology*. 11 July 2015. Vol. 29, no. 7, p. 2803–2815. DOI 10.1007/s12206-015-0609-9.

APPENDIX

I. THE COVER PAGE OF PUBLISHED ARTICLE

1613(16600) *ISSN 1392–1207. MECHANIKA. 2016 Volume 22(6): 8–1*

Vibrational and numerical evaluation of human incus mechanical properties

V. Gylienė*, N. Kraptavičiūtė*, P. Lipinski, S. Wronski***, R. Rahouadj****, J. Tarasiuk***, A. Baldit**, G. Gylys*****, K. Norkaitytė*******

*Kaunas University of Technology, Studentų 56, LT-51424 Kaunas, Lithuania,
E-mail: virginija.gyliene@ktu.lt, neringa.kraptaviciute@ktu.edu
***University of Lorraine, ENIM - LaBPS, 1 route d'Ars Laquenexy, FR-57078 Metz Cedex 3, France,*
E-mail: pawel.lipinski@univ-lorraine.fr, adrien.baldit@univ-lorraine.fr
**** AGH University of Science and Technology, Al Mickiewicza 30, PL-30059 Krakow, Poland,*
E-mail: wronski.sebastian@gmail.com, tarasiuk@agh.edu.pl
*****University of Lorraine, LEMTA, 2 Ave Foret Haye,TSA 60604, F-54518 Vandoeuvre Les Nancy, France,*
E-mail: rachid.rahouadj@univ-lorraine.fr
******Lithuanian University of Health Sciences, Department of Oto-Rhino-Laryngology, Eivenių 2, LT-50009 Kaunas, Lithuania, E-mail: gylysg@yahoo.com, nork.kristina@gmail.com*

1. Introduction

The mechanism of hearing involves conduction of mechanical vibrations along the ossicular chain to the inner ear [1]. The middle ear system with its smallest bones and articulations is responsible for catching noise energy and transforming it to perilymph pressure changes in the cochlea. The ossicular chain (the malleus, the incus and the stapes - Fig. 1) connects the tympanic membrane and the inner ear, and plays an important role in amplifying and regulating sound waves [2]. In doing so the spatial motion of the ossicular chain appears as the one of main causes of the hearing quality [3].

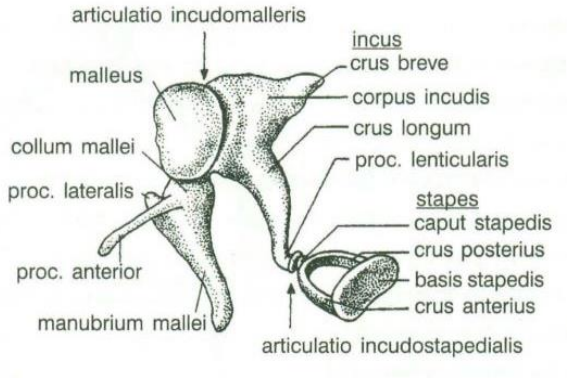

Fig. 1 The ossicular chain of human ear [4]

The degree of ossicular chain deterioration or damage in humans, as a result of inflammatory disease, trauma or malformation, is variable [5]. Of the three ossicles from the middle ear, the incus was often reported in literature to be the most eroded bone and the more distant from the inflammation focus [6, 7]. Borgstein et al [8] highlighted, that the problem of erosion of the incus is a frequently observed, but rarely discussed problem. Park [9] also examined the problems of the long process of incus but caused by congenital origin. Finally, Yuang [10] summarised ossicular damage in the patients with atelectasis and found that for 72% of cases in posterior retraction pocket only incus was eroded.

There are many ways to reconstruct the ossicular chain, but the results are not always satisfactory because it is being done usually by columella (bird) effect, which sometimes is unsatisfactory for hearing impairment. Sometimes, some artificial materials, as glue [11] for example, could be used to reconstruct the ossicular chain discontinuity. Or the use of glass ionomer cement to repair incus long process defects is a suitable method that improves hearing in pediatric patients [12]. It is hypothesised that the function of the malleus-incus-stapes arrangement is to link the drum to the oval window with the flexibility required for impedance matching but the rigidity to prevent unconstrainable resonances from occurring in the hearing range [1]. If it is true, then the structural stiffness of ossicular chain is the critical design for middle-ear replacement prostheses.

Nevertheless, the substituting materials should fit according to the material characteristics; the geometrical requirements are also important. Kaftan et al [5] accentuate that the most difficult situation is to evaluate the length of prosthesis. For this kind of problems, and others, the finite element method (FEM) has distinct advantages in modelling complex biological systems when compared to other techniques [13]. Even, as reported in [14], it could improve the clinical surgical intervention.

Consecutively to ossicles' surgery, the surgeons are observing that incus bone work does not depend only on degradation level and affected area size. It was also observed that sometimes damaged bone part is large but it does not affect bone work in whole hearing system and opposite – the bone degradation level can be low but the ossicles not functioning well.

KAUNO TECHNOLOGIJOS UNIVERSITETO
MECHANIKOS INŽINERIJOS IR DIZAINO FAKULTETAS

Žurnalo „Mechanika“ atsakingasis sekretorius
Saulius Diliūnas

Dėl mokslinio straipsnio pateikimo
moksliniam žurnalui „Mechanika“

PAŽYMA

2016-11-21
Kaunas

Pažymime, kad *V. Gylienė*, *N. Kraptavičiūtė*, *P. Lipinski*, *A. Baldit*, *S. Wronski*, *J. Tarasiuk*, *R. Rahouadj*, *G. Gylys* ir *K. Norkaitytė* mokslinio žurnalo „Mechanika“ redakcijai pateikė straipsnį „*Vibrational and numerical evaluation of human incus mechanical properties*“. Straipsnis apiformintas pagal keliamus reikalavimus. Atsiliepimas teigiamas. Straipsnis ruošiamas spaudai. Planuojama spausdinti šių metų „Mechanika“ 22(6) leidinyje.

Mokslinio žurnalo „Mechanika“ atsakingasis sekretorius
Saulius Diliūnas

Saulius Diliūnas, tel. (8 685) 96413, el. p. Saulius.Diliunas@ktu.lt

II. DISPLACEMENT DIAGRAMS

I.I. LINEAR ELEMENT TYPE

LINEAR ELEMENT TYPE			
Type of el.	**MODE No.**	**Original *1M* sample**	**„Healthy" bone model**
157	0	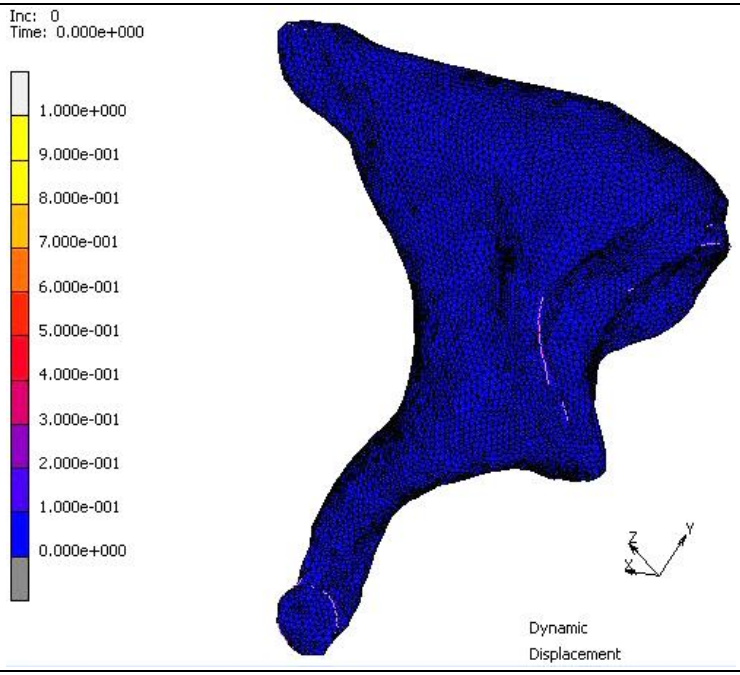	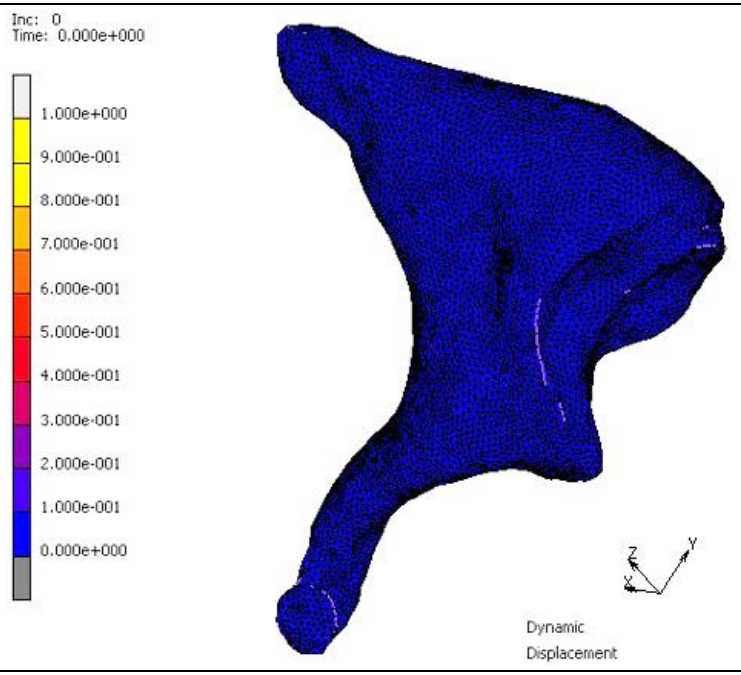

157	1	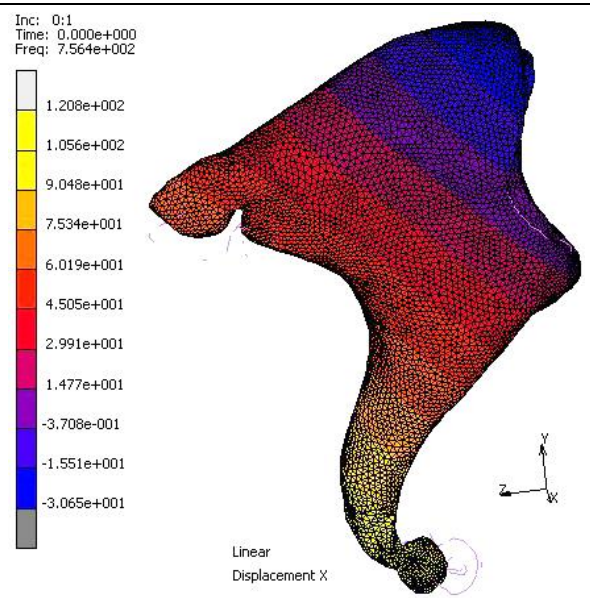 Inc: 0:1 Time: 0.000e+000 Freq: 7.564e+002 1.208e+002 1.056e+002 9.048e+001 7.534e+001 6.019e+001 4.505e+001 2.991e+001 1.477e+001 -3.708e-001 -1.551e+001 -3.065e+001 Linear Displacement X	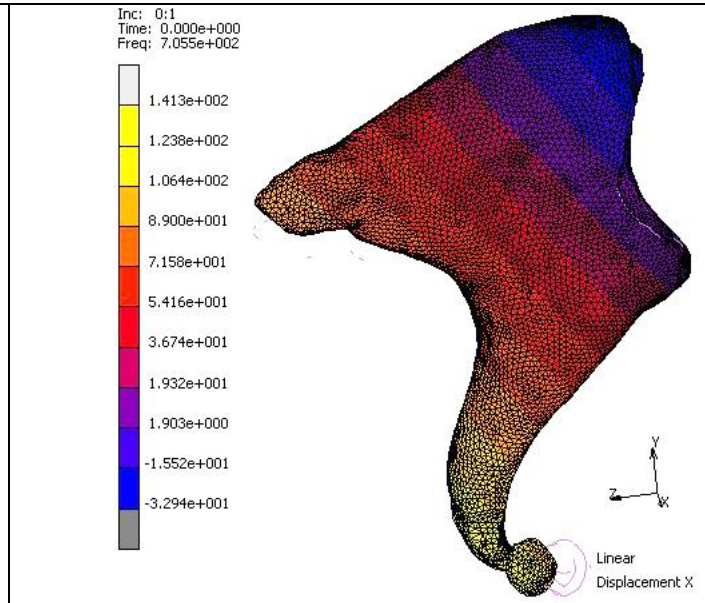 Inc: 0:1 Time: 0.000e+000 Freq: 7.055e+002 1.413e+002 1.238e+002 1.064e+002 8.900e+001 7.158e+001 5.416e+001 3.674e+001 1.932e+001 1.903e+000 -1.552e+001 -3.294e+001 Linear Displacement X
157	2	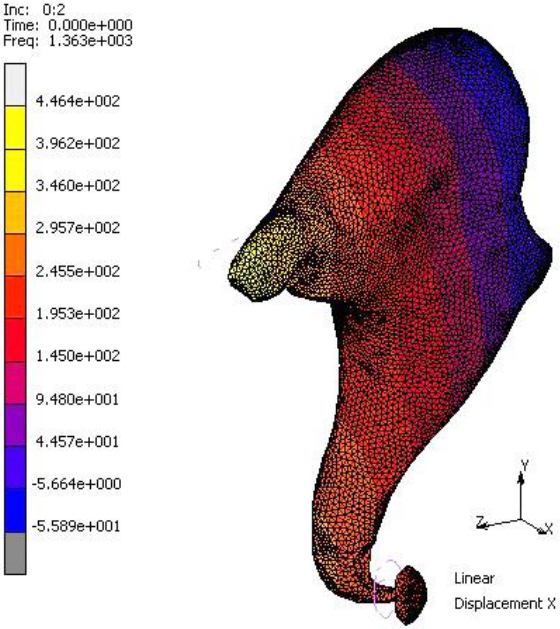 Inc: 0:2 Time: 0.000e+000 Freq: 1.363e+003 4.464e+002 3.962e+002 3.460e+002 2.957e+002 2.455e+002 1.953e+002 1.450e+002 9.480e+001 4.457e+001 -5.664e+000 -5.589e+001 Linear Displacement X	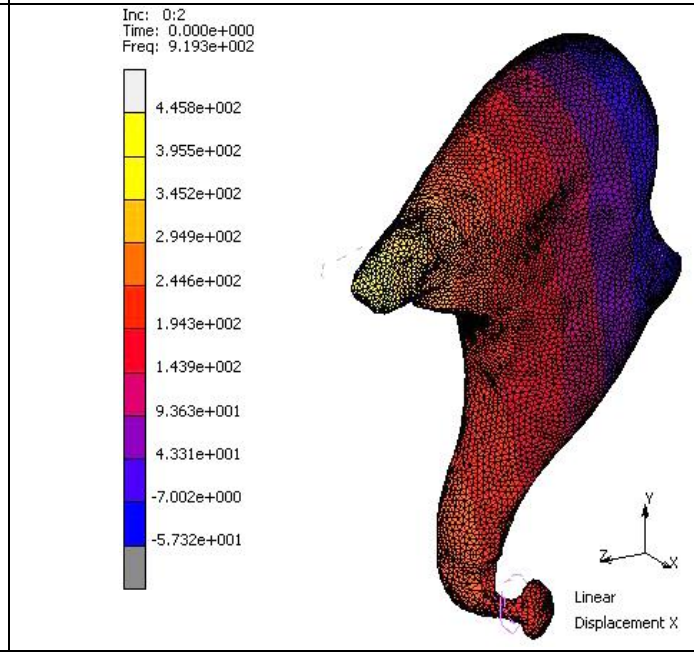 Inc: 0:2 Time: 0.000e+000 Freq: 9.193e+002 4.458e+002 3.955e+002 3.452e+002 2.949e+002 2.446e+002 1.943e+002 1.439e+002 9.363e+001 4.331e+001 -7.002e+000 -5.732e+001 Linear Displacement X

157	3	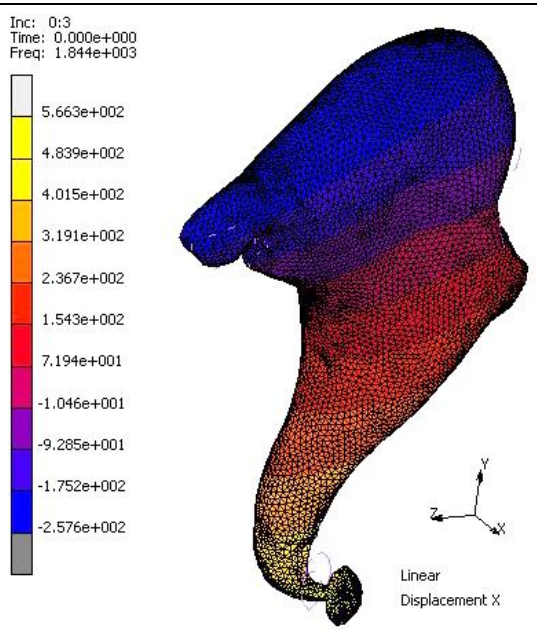 Inc: 0:3 Time: 0.000e+000 Freq: 1.844e+003 5.663e+002 4.839e+002 4.015e+002 3.191e+002 2.367e+002 1.543e+002 7.194e+001 -1.046e+001 -9.285e+001 -1.752e+002 -2.576e+002 Y Z X Linear Displacement X	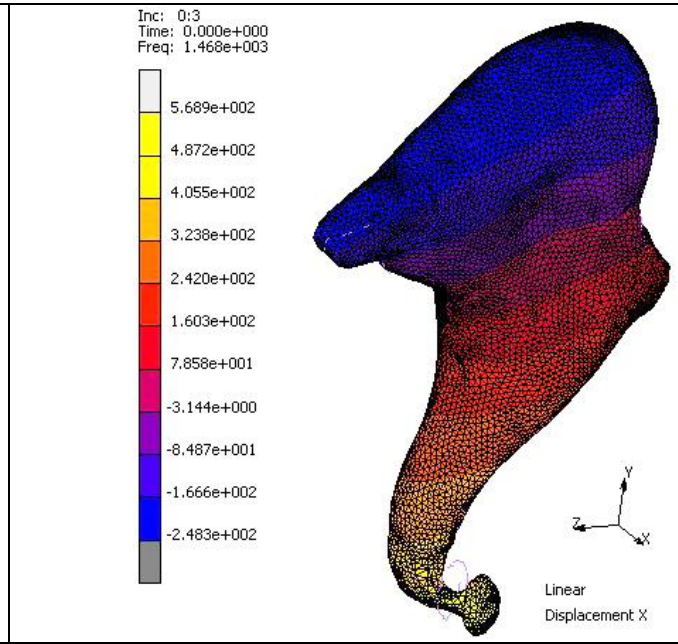 Inc: 0:3 Time: 0.000e+000 Freq: 1.468e+003 5.689e+002 4.872e+002 4.055e+002 3.238e+002 2.420e+002 1.603e+002 7.858e+001 -3.144e+000 -8.487e+001 -1.666e+002 -2.483e+002 Y Z X Linear Displacement X
157	4	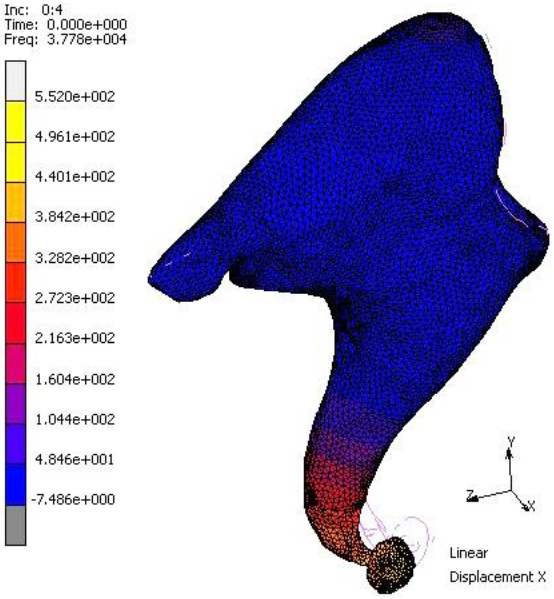 Inc: 0:4 Time: 0.000e+000 Freq: 3.778e+004 5.520e+002 4.961e+002 4.401e+002 3.842e+002 3.282e+002 2.723e+002 2.163e+002 1.604e+002 1.044e+002 4.846e+001 -7.486e+000 Y Z X Linear Displacement X	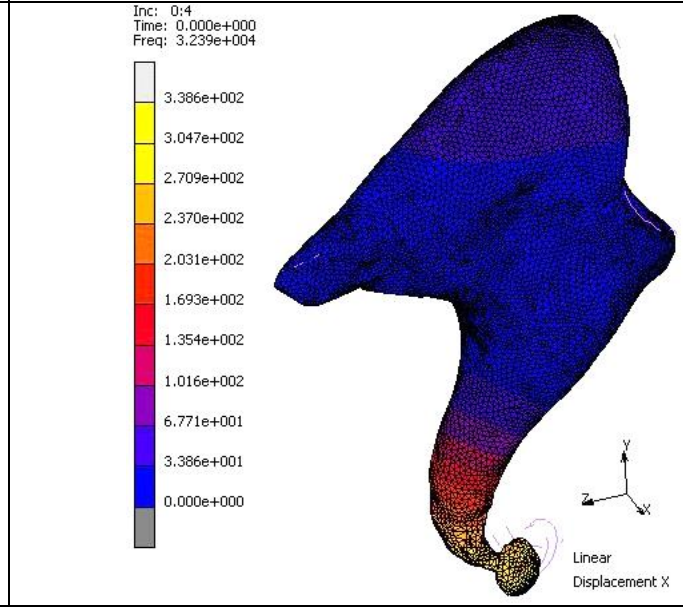 Inc: 0:4 Time: 0.000e+000 Freq: 3.239e+004 3.386e+002 3.047e+002 2.709e+002 2.370e+002 2.031e+002 1.693e+002 1.354e+002 1.016e+002 6.771e+001 3.386e+001 0.000e+000 Y Z X Linear Displacement X

157	5	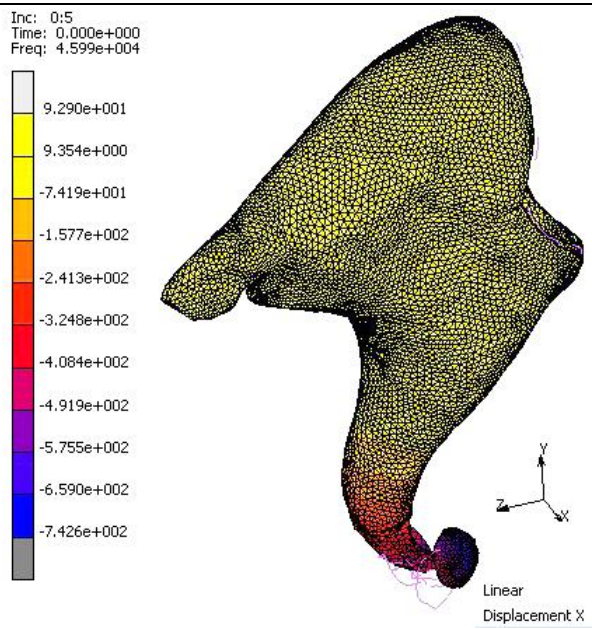 Inc: 0:5 Time: 0.000e+000 Freq: 4.599e+004 9.290e+001 9.354e+000 -7.419e+001 -1.577e+002 -2.413e+002 -3.248e+002 -4.084e+002 -4.919e+002 -5.755e+002 -6.590e+002 -7.426e+002 Linear Displacement X	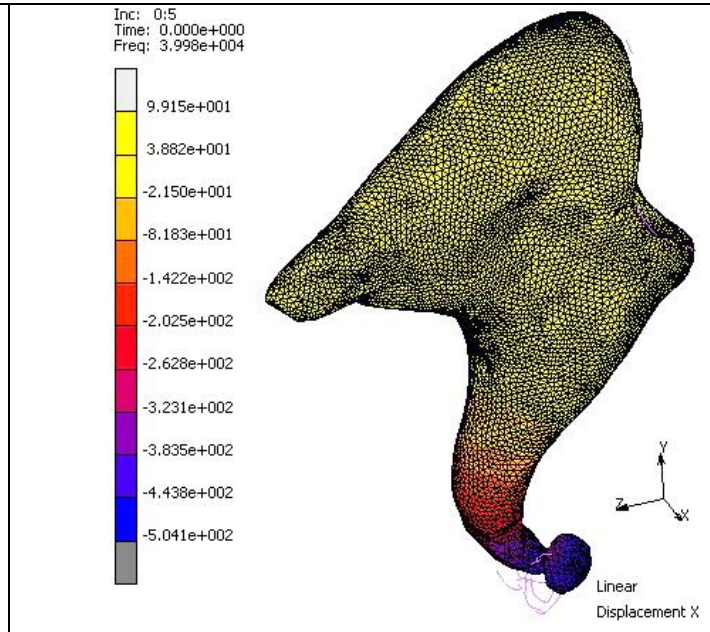 Inc: 0:5 Time: 0.000e+000 Freq: 3.998e+004 9.915e+001 3.882e+001 -2.150e+001 -8.183e+001 -1.422e+002 -2.025e+002 -2.628e+002 -3.231e+002 -3.835e+002 -4.438e+002 -5.041e+002 Linear Displacement X
157	6	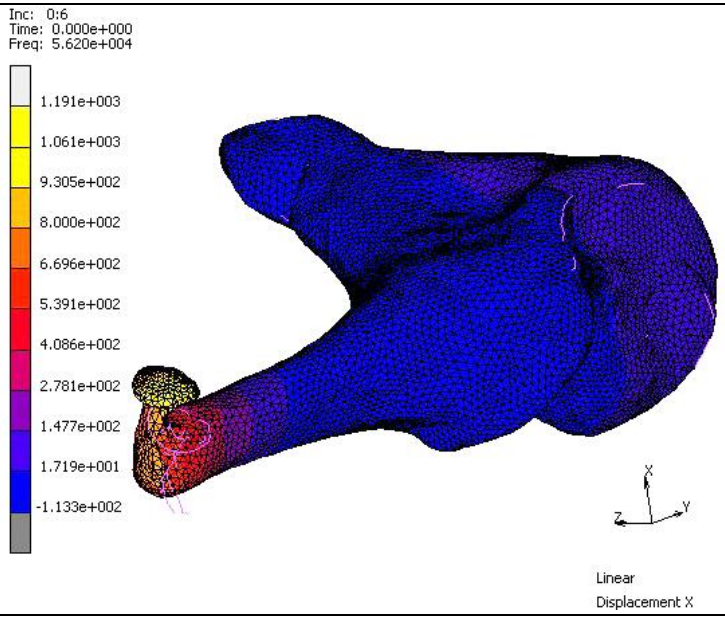 Inc: 0:6 Time: 0.000e+000 Freq: 5.620e+004 1.191e+003 1.061e+003 9.305e+002 8.000e+002 6.696e+002 5.391e+002 4.086e+002 2.781e+002 1.477e+002 1.719e+001 -1.133e+002 Linear Displacement X	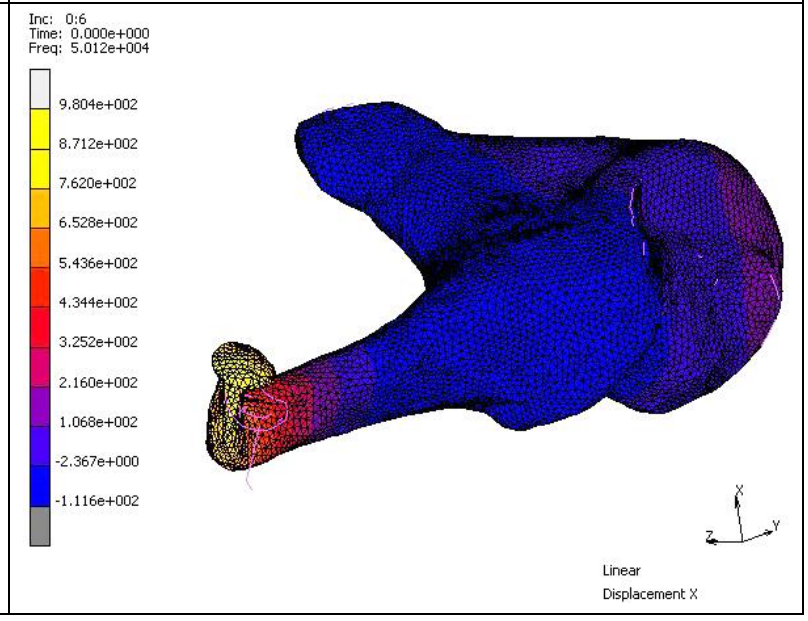 Inc: 0:6 Time: 0.000e+000 Freq: 5.012e+004 9.804e+002 8.712e+002 7.620e+002 6.528e+002 5.436e+002 4.344e+002 3.252e+002 2.160e+002 1.068e+002 -2.367e+000 -1.116e+002 Linear Displacement X

157	7	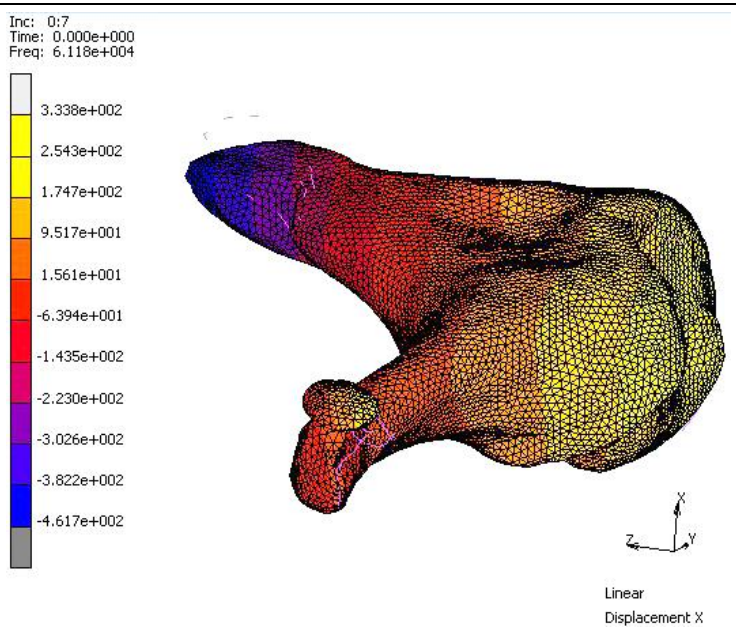 Inc: 0:7 Time: 0.000e+000 Freq: 6.118e+004 3.338e+002 2.543e+002 1.747e+002 9.517e+001 1.561e+001 -6.394e+001 -1.435e+002 -2.230e+002 -3.026e+002 -3.822e+002 -4.617e+002 Linear Displacement X	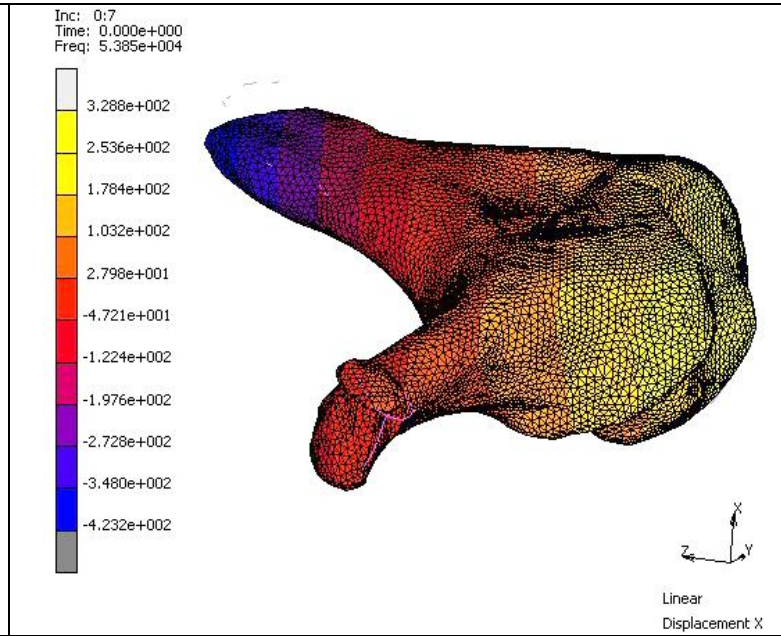 Inc: 0:7 Time: 0.000e+000 Freq: 5.385e+004 3.288e+002 2.536e+002 1.784e+002 1.032e+002 2.798e+001 -4.721e+001 -1.224e+002 -1.976e+002 -2.728e+002 -3.480e+002 -4.232e+002 Linear Displacement X
157	8	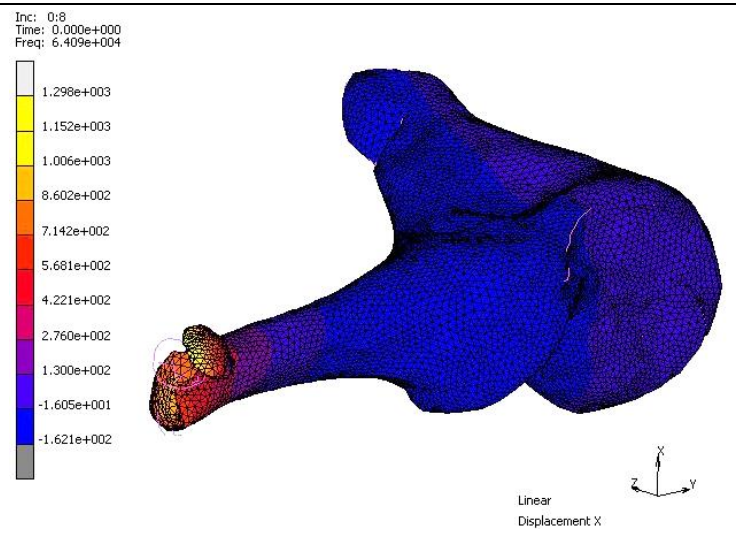 Inc: 0:8 Time: 0.000e+000 Freq: 6.409e+004 1.298e+003 1.152e+003 1.006e+003 8.602e+002 7.142e+002 5.681e+002 4.221e+002 2.760e+002 1.300e+002 -1.605e+001 -1.621e+002 Linear Displacement X	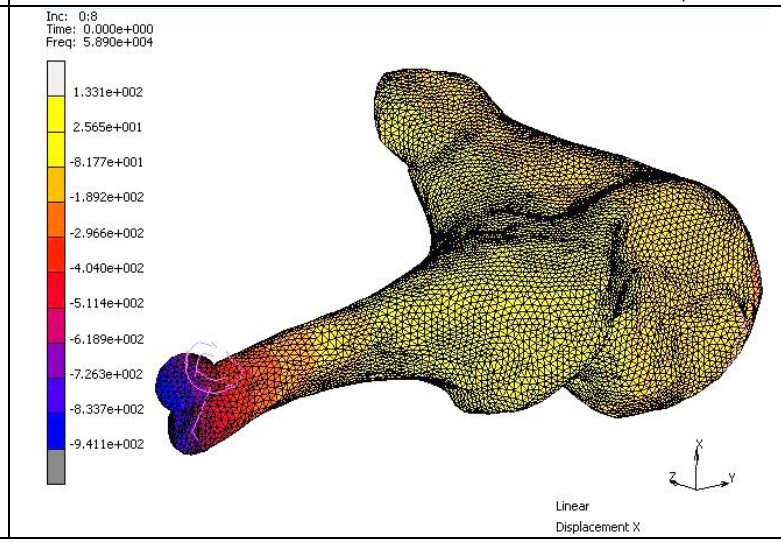 Inc: 0:8 Time: 0.000e+000 Freq: 5.890e+004 1.331e+002 2.565e+001 -8.177e+001 -1.892e+002 -2.966e+002 -4.040e+002 -5.114e+002 -6.189e+002 -7.263e+002 -8.337e+002 -9.411e+002 Linear Displacement X

157	9	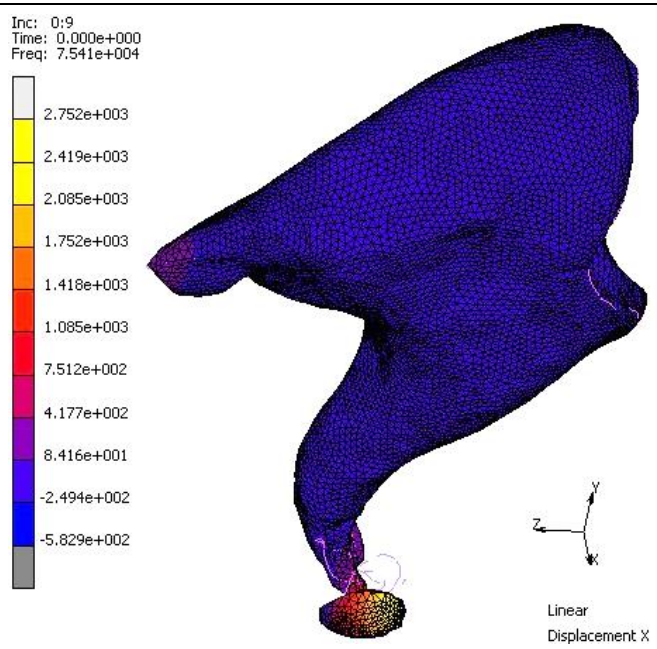 Inc: 0:9 Time: 0.000e+000 Freq: 7.541e+004 2.752e+003 2.419e+003 2.085e+003 1.752e+003 1.418e+003 1.085e+003 7.512e+002 4.177e+002 8.416e+001 -2.494e+002 -5.829e+002 Linear Displacement X	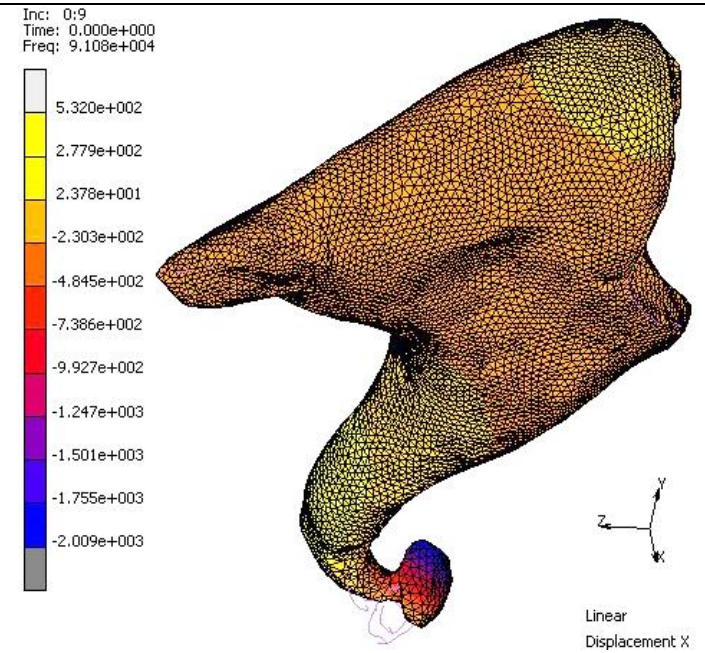 Inc: 0:9 Time: 0.000e+000 Freq: 9.108e+004 5.320e+002 2.779e+002 2.378e+001 -2.303e+002 -4.845e+002 -7.386e+002 -9.927e+002 -1.247e+003 -1.501e+003 -1.755e+003 -2.009e+003 Linear Displacement X
157	10	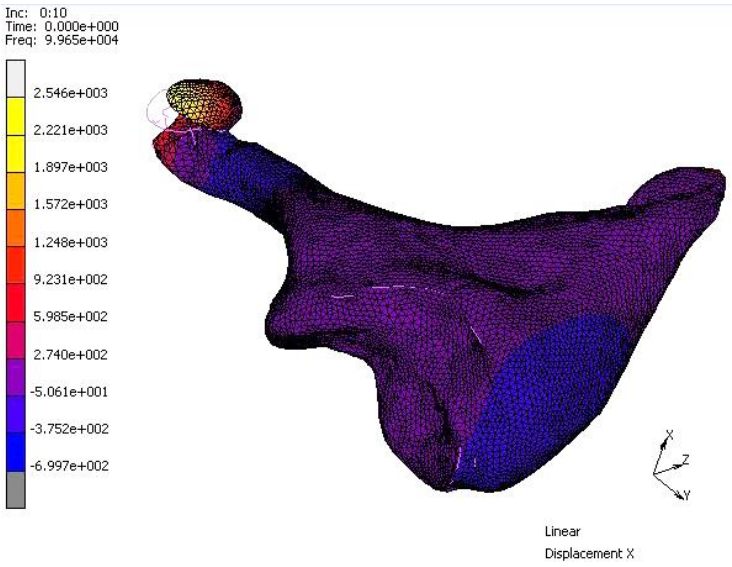 Inc: 0:10 Time: 0.000e+000 Freq: 9.965e+004 2.546e+003 2.221e+003 1.897e+003 1.572e+003 1.248e+003 9.231e+002 5.985e+002 2.740e+002 -5.061e+001 -3.752e+002 -6.997e+002 Linear Displacement X	Inc: 0:10 Time: 0.000e+000 Freq: 1.022e+005 5.958e+002 3.841e+002 1.724e+002 -3.932e+001 -2.510e+002 -4.627e+002 -6.744e+002 -8.861e+002 -1.098e+003 -1.309e+003 -1.521e+003 Linear Displacement X

I.II. QUADRATIC ELEMENT TYPE

QUADRATIC ELEMENT TYPE			
Type of el.	**MODE No.**	**Original *1M* sample**	**„Healthy" bone model**
127	1	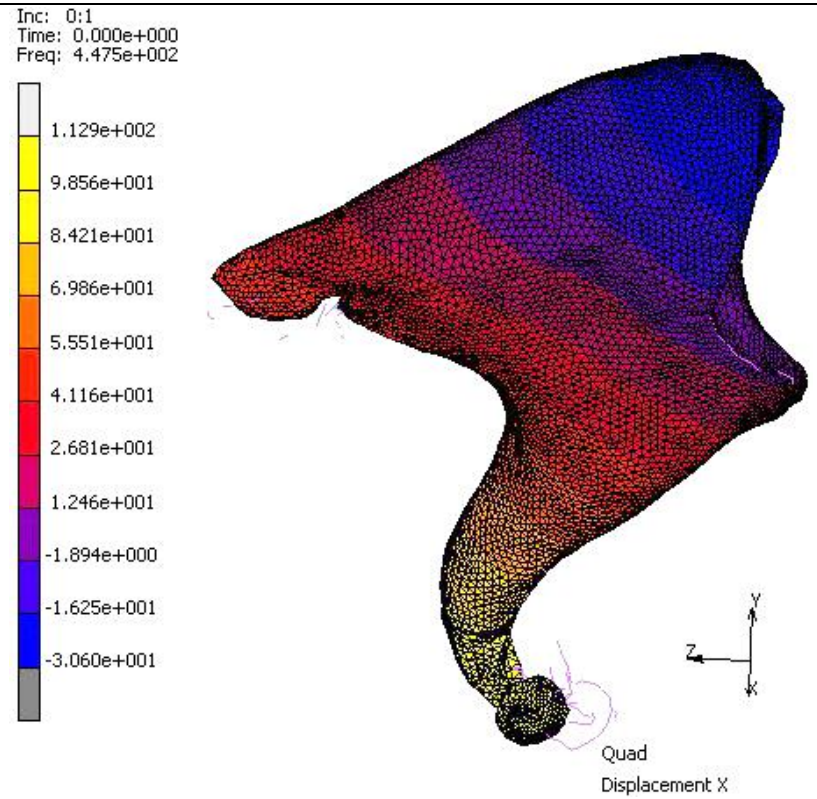	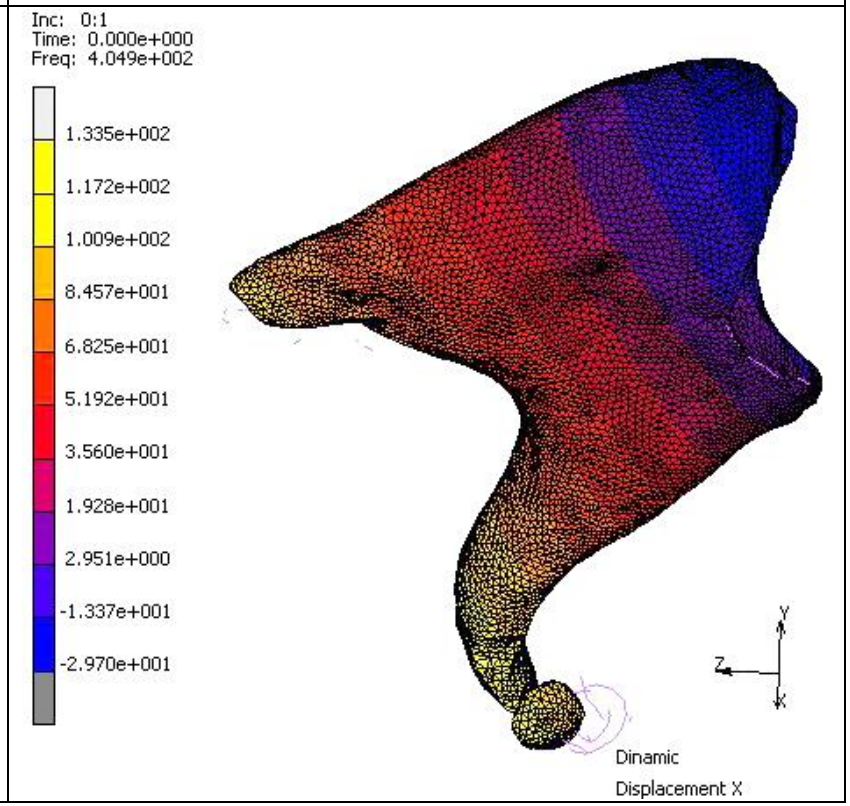

127	2	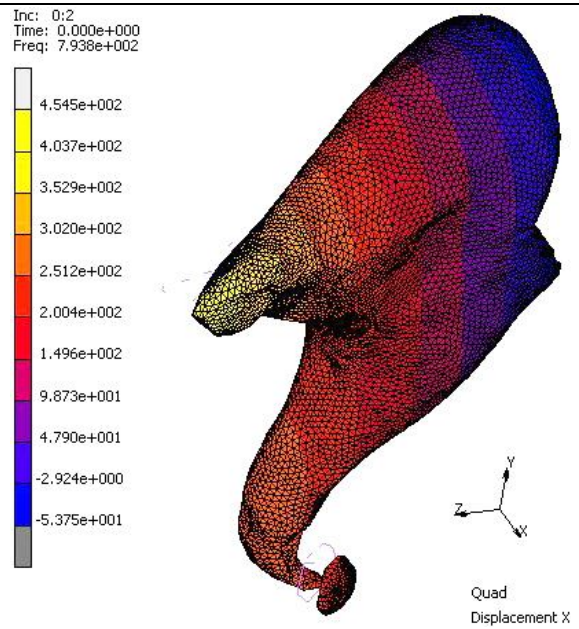 Inc: 0:2 Time: 0.000e+000 Freq: 7.938e+002 4.545e+002 4.037e+002 3.529e+002 3.020e+002 2.512e+002 2.004e+002 1.496e+002 9.873e+001 4.790e+001 -2.924e+000 -5.375e+001 Quad Displacement X	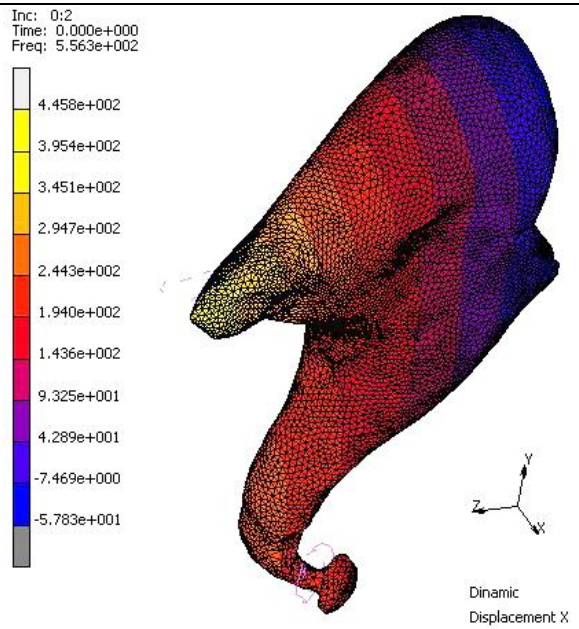 Inc: 0:2 Time: 0.000e+000 Freq: 5.563e+002 4.458e+002 3.954e+002 3.451e+002 2.947e+002 2.443e+002 1.940e+002 1.436e+002 9.325e+001 4.289e+001 -7.469e+000 -5.783e+001 Dinamic Displacement X
127	3	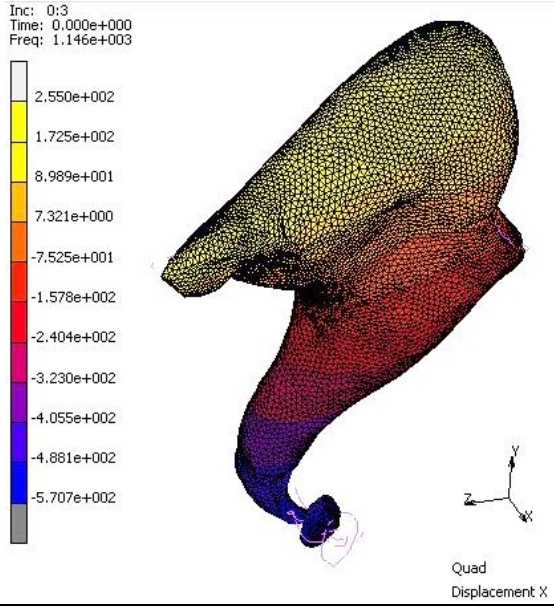 Inc: 0:3 Time: 0.000e+000 Freq: 1.146e+003 2.550e+002 1.725e+002 8.989e+001 7.321e+000 -7.525e+001 -1.578e+002 -2.404e+002 -3.230e+002 -4.055e+002 -4.881e+002 -5.707e+002 Quad Displacement X	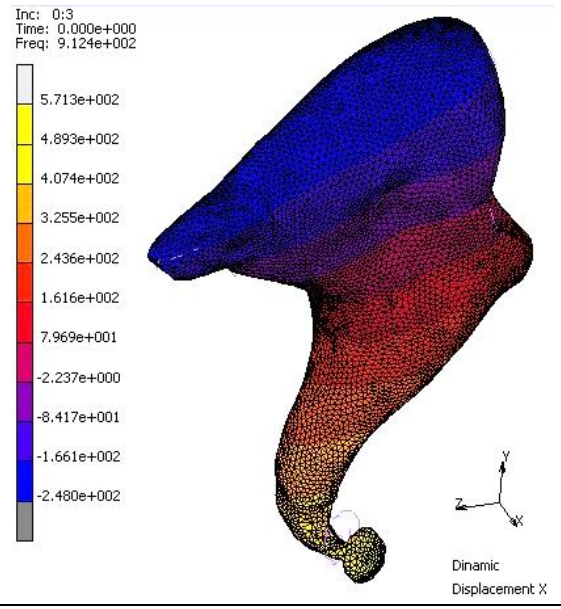 Inc: 0:3 Time: 0.000e+000 Freq: 9.124e+002 5.713e+002 4.893e+002 4.074e+002 3.255e+002 2.436e+002 1.616e+002 7.969e+001 -2.237e+000 -8.417e+001 -1.661e+002 -2.480e+002 Dinamic Displacement X

127	4	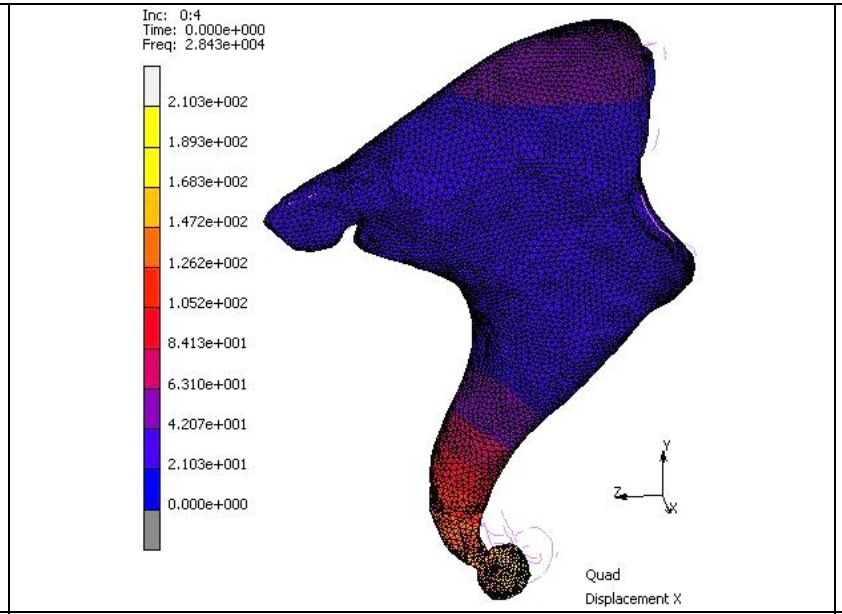 Inc: 0:4 Time: 0.000e+000 Freq: 2.843e+004 2.103e+002 1.893e+002 1.683e+002 1.472e+002 1.262e+002 1.052e+002 8.413e+001 6.310e+001 4.207e+001 2.103e+001 0.000e+000 Quad Displacement X	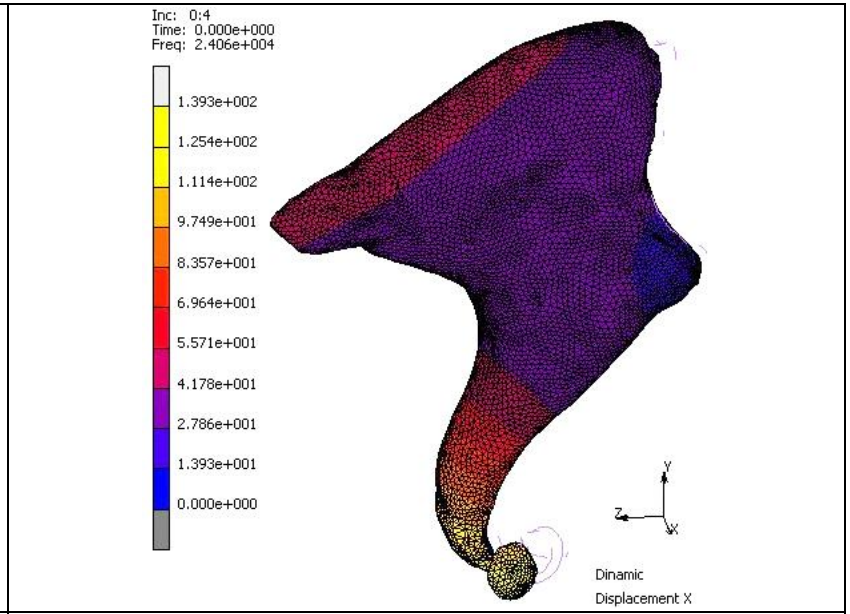 Inc: 0:4 Time: 0.000e+000 Freq: 2.406e+004 1.393e+002 1.254e+002 1.114e+002 9.749e+001 8.357e+001 6.964e+001 5.571e+001 4.178e+001 2.786e+001 1.393e+001 0.000e+000 Dinamic Displacement X
127	5	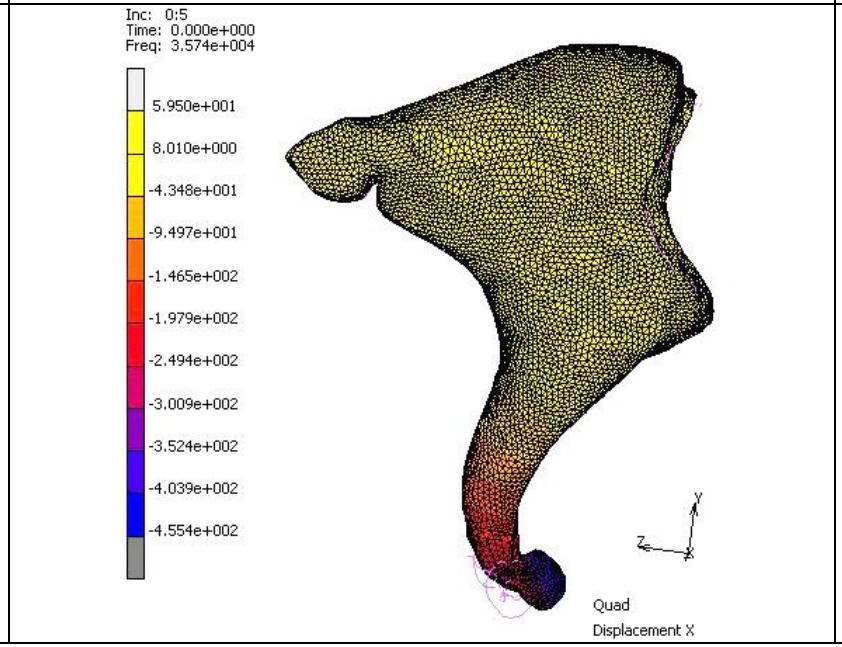 Inc: 0:5 Time: 0.000e+000 Freq: 3.574e+004 5.950e+001 8.010e+000 -4.348e+001 -9.497e+001 -1.465e+002 -1.979e+002 -2.494e+002 -3.009e+002 -3.524e+002 -4.039e+002 -4.554e+002 Quad Displacement X	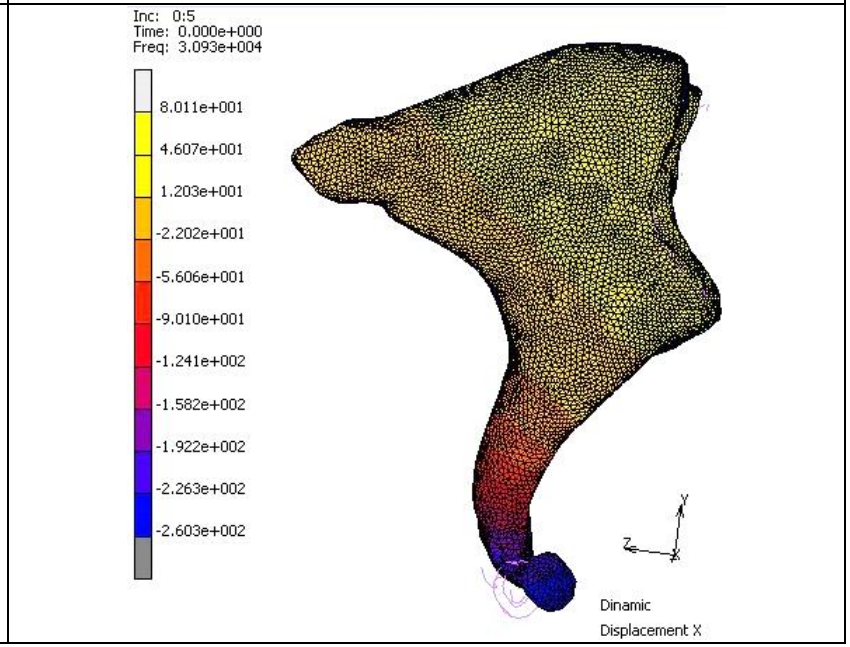 Inc: 0:5 Time: 0.000e+000 Freq: 3.093e+004 8.011e+001 4.607e+001 1.203e+001 -2.202e+001 -5.606e+001 -9.010e+001 -1.241e+002 -1.582e+002 -1.922e+002 -2.263e+002 -2.603e+002 Dinamic Displacement X

127	6	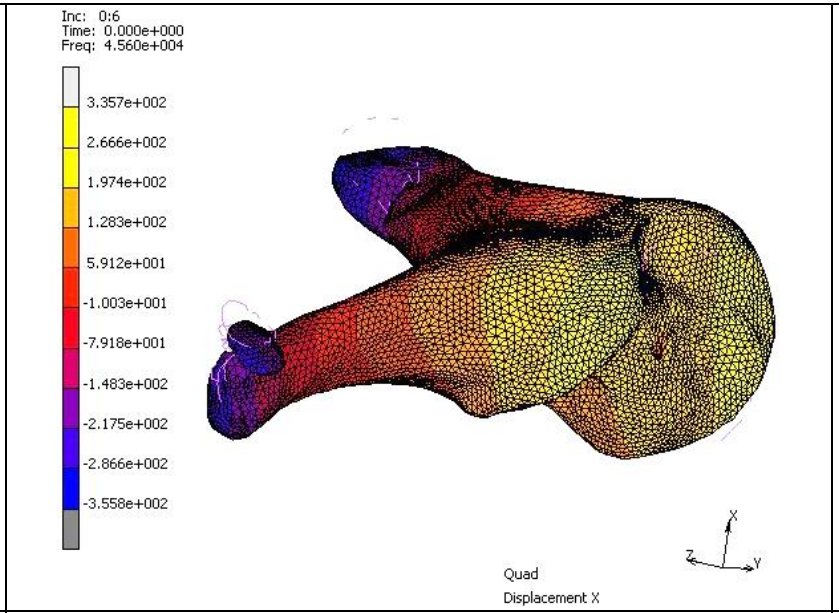 Inc: 0:6 Time: 0.000e+000 Freq: 4.560e+004 3.357e+002 2.666e+002 1.974e+002 1.283e+002 5.912e+001 -1.003e+001 -7.918e+001 -1.483e+002 -2.175e+002 -2.866e+002 -3.558e+002 Quad Displacement X	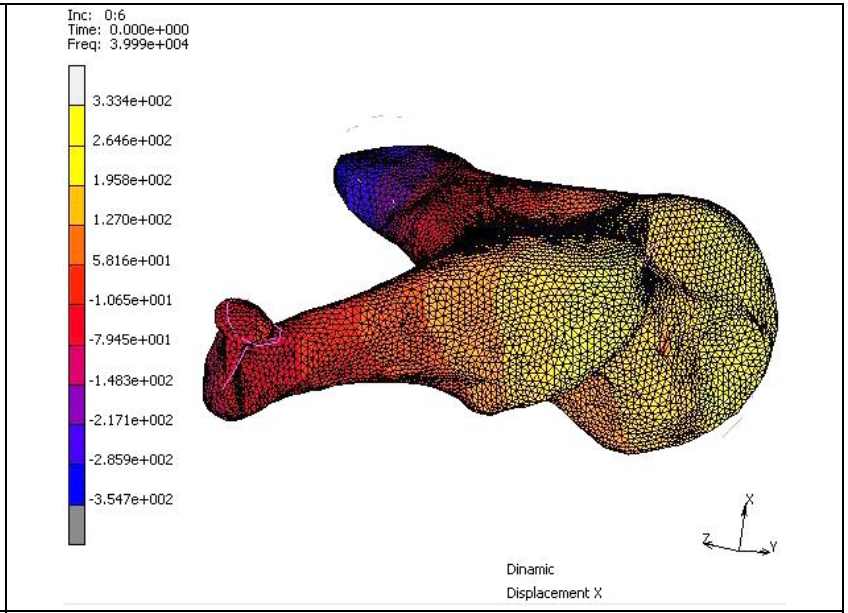 Inc: 0:6 Time: 0.000e+000 Freq: 3.999e+004 3.334e+002 2.646e+002 1.958e+002 1.270e+002 5.816e+001 -1.065e+001 -7.945e+001 -1.483e+002 -2.171e+002 -2.859e+002 -3.547e+002 Dinamic Displacement X
127	7	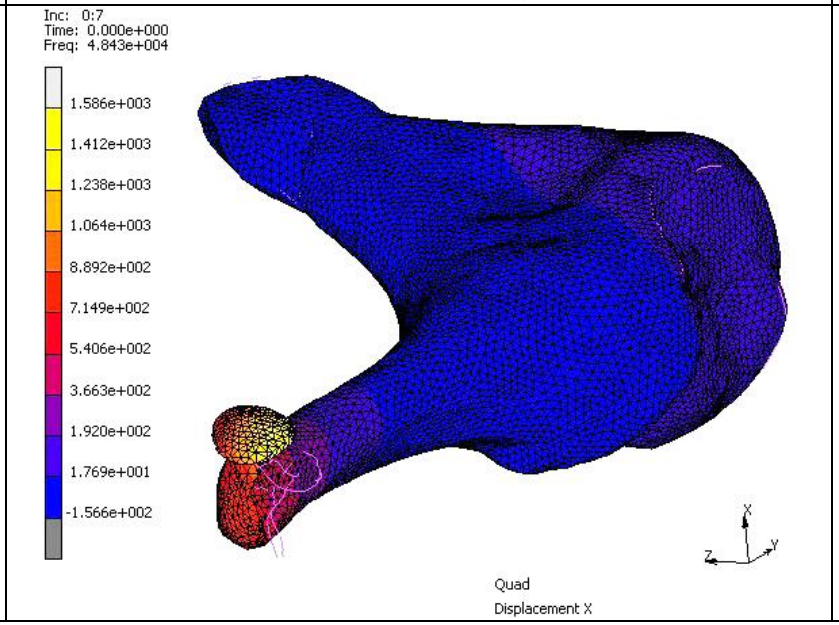 Inc: 0:7 Time: 0.000e+000 Freq: 4.843e+004 1.586e+003 1.412e+003 1.238e+003 1.064e+003 8.892e+002 7.149e+002 5.406e+002 3.663e+002 1.920e+002 1.769e+001 -1.566e+002 Quad Displacement X	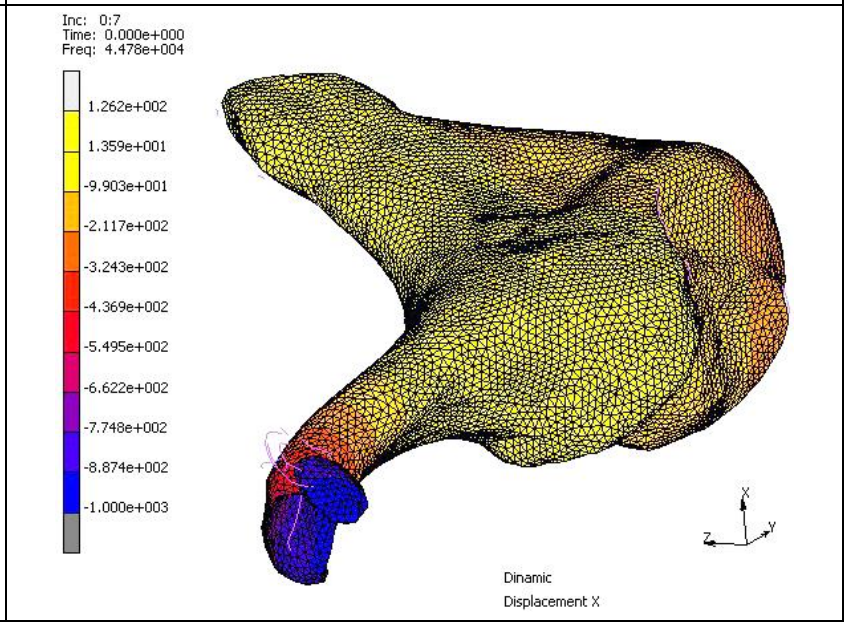 Inc: 0:7 Time: 0.000e+000 Freq: 4.478e+004 1.262e+002 1.359e+001 -9.903e+001 -2.117e+002 -3.243e+002 -4.369e+002 -5.495e+002 -6.622e+002 -7.748e+002 -8.874e+002 -1.000e+003 Dinamic Displacement X

127	8	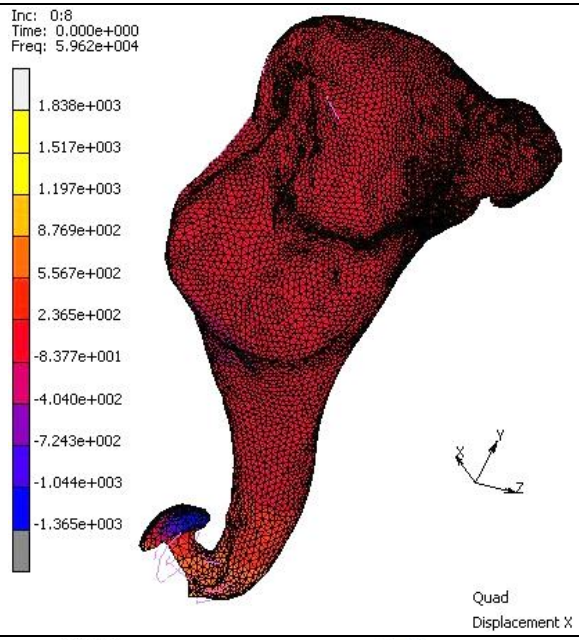 Inc: 0:8 Time: 0.000e+000 Freq: 5.962e+004 1.838e+003 1.517e+003 1.197e+003 8.769e+002 5.567e+002 2.365e+002 -8.377e+001 -4.040e+002 -7.243e+002 -1.044e+003 -1.365e+003 Quad Displacement X	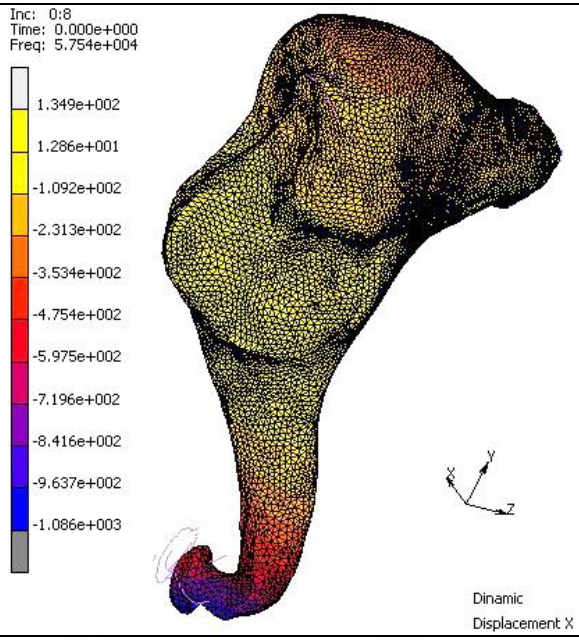 Inc: 0:8 Time: 0.000e+000 Freq: 5.754e+004 1.349e+002 1.286e+001 -1.092e+002 -2.313e+002 -3.534e+002 -4.754e+002 -5.975e+002 -7.196e+002 -8.416e+002 -9.637e+002 -1.086e+003 Dinamic Displacement X
127	9	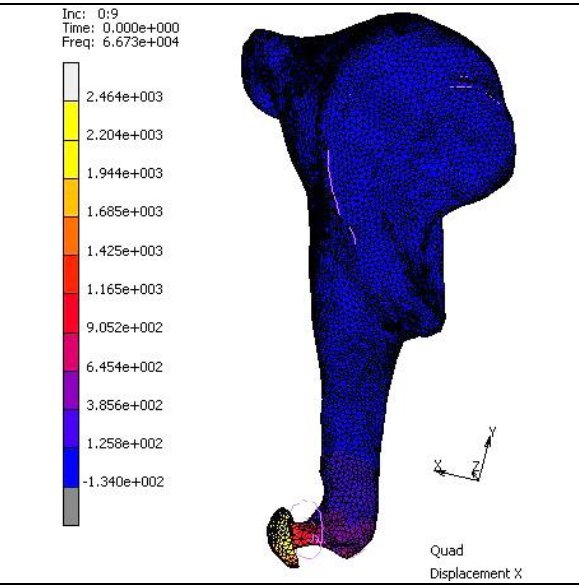 Inc: 0:9 Time: 0.000e+000 Freq: 6.673e+004 2.464e+003 2.204e+003 1.944e+003 1.685e+003 1.425e+003 1.165e+003 9.052e+002 6.454e+002 3.856e+002 1.258e+002 -1.340e+002 Quad Displacement X	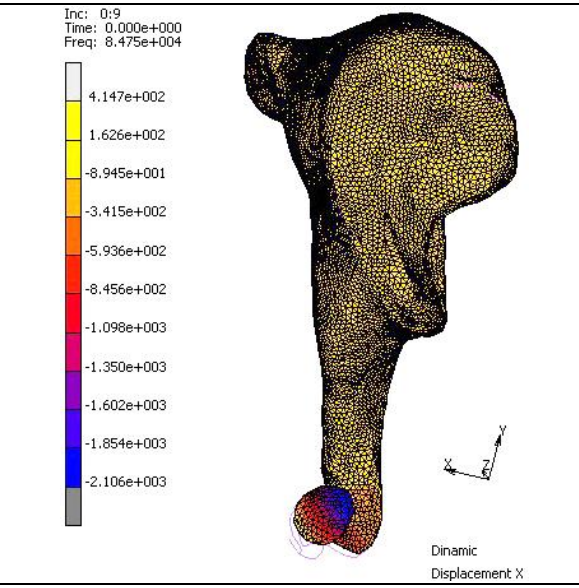 Inc: 0:9 Time: 0.000e+000 Freq: 8.475e+004 4.147e+002 1.626e+002 -8.945e+001 -3.415e+002 -5.936e+002 -8.456e+002 -1.098e+003 -1.350e+003 -1.602e+003 -1.854e+003 -2.106e+003 Dinamic Displacement X

127	10	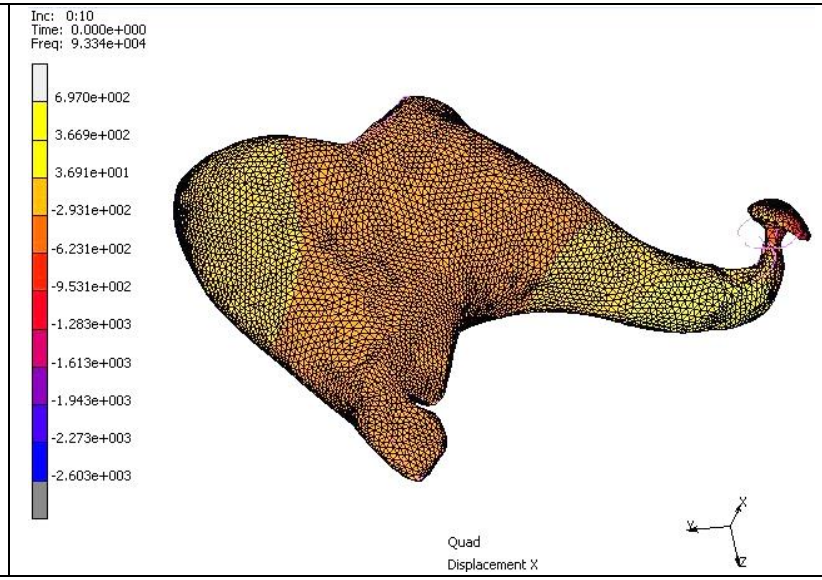 Inc: 0:10 Time: 0.000e+000 Freq: 9.334e+004 6.970e+002 3.669e+002 3.691e+001 -2.931e+002 -6.231e+002 -9.531e+002 -1.283e+003 -1.613e+003 -1.943e+003 -2.273e+003 -2.603e+003 Quad Displacement X	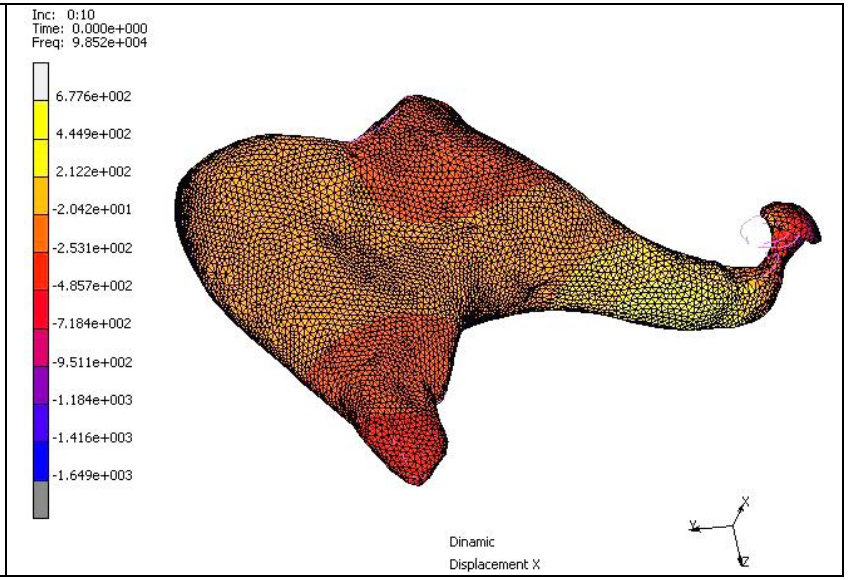 Inc: 0:10 Time: 0.000e+000 Freq: 9.852e+004 6.776e+002 4.449e+002 2.122e+002 -2.042e+001 -2.531e+002 -4.857e+002 -7.184e+002 -9.511e+002 -1.184e+003 -1.416e+003 -1.649e+003 Dinamic Displacement X